

## Paleoseismic evidence of great surface rupture earthquakes along the Indian Himalaya

Senthil Kumar,<sup>1</sup> Steven G. Wesnousky,<sup>1</sup> Thomas K. Rockwell,<sup>2</sup> Richard W. Briggs,<sup>1</sup> Vikram C. Thakur,<sup>3</sup> and R. Jayangondaperumal<sup>3</sup>

Received 8 July 2004; revised 8 July 2005; accepted 12 October 2005; published 8 March 2006.

[1] Toward understanding the relationship between strain accumulation and strain release in the context of the mechanics of the earthquake and mountain building process and quantifying the seismic hazard associated with the globe's largest continental thrust system, we describe the late Quaternary expression and paleoseismic evidence for great surface rupture earthquakes at six sites along the Himalayan Frontal Thrust (HFT) system of India. Our observations span a distance of  $\sim 250$  km along strike of the HFT. Uplifted and truncated fluvial terrace deposits resulting from the Holocene displacements on the HFT are preserved along canyons of the Ghaggar, Markanda, Shajahanpur, and Kosi Rivers. Dividing the elevation of the bedrock straths at each site by their ages yields estimates of the vertical uplift rate of  $\sim 4$ – $6$  mm/yr, which when assumed to be the result of slip on an underlying thrust dipping at  $\sim 20^\circ$ – $45^\circ$  are equivalent to fault slip rates of  $\sim 6$ – $18$  mm/yr or shortening rates of  $\sim 4$ – $16$  mm/yr. Trench exposures reveal the HFT to fold and break late Holocene surface sediments near the cities and villages of Chandigarh, Kala Amb, Rampur Ganda, Lal Dhang, and Ramnagar. Radiocarbon ages of samples obtained from the displaced sediments indicate surface rupture at each site took place after  $\sim$ A.D. 1200 and before  $\sim$ A.D. 1700. Uncertainties attendant to the radiocarbon dating currently do not allow an unambiguous definition of the capping bound on the age of the displacement at each site and hence whether or not the displacements at all sites were contemporaneous. Trench exposures and vertical separations measured across scarps at Rampur Ganda, Lal Dhang, and Ramnagar are interpreted to indicate single-event displacements of  $\sim 11$ – $38$  m. Dividing the observed single-event vertical components of displacement by the estimated longer-term uplift rates indicates  $\sim 1330$ – $3250$  or more years should be required to accumulate the slip sufficient to produce similar sized displacements. Surface rupture appears to not have occurred during the historical 1905 Kangra ( $M_w = 7.7$ ), 1934 Bihar-Nepal ( $M_w = 8.1$ ), and 1950 Assam ( $M_w = 8.4$ ) earthquakes, which also occurred along the Himalayan front. Yet we observe clear evidence of fault scarps and displacements in young alluvium and progressive and continued offset of fluvial terrace deposits along the HFT. We suggest on this basis and the size and possible synchronicity of displacements recorded in the trenches that there exists the potential for earthquakes larger than recorded in the historical record and with the potential to rupture lengths of the HFT greater than the  $\sim 250$  km we have studied.

**Citation:** Kumar, S., S. G. Wesnousky, T. K. Rockwell, R. W. Briggs, V. C. Thakur, and R. Jayangondaperumal (2006), Paleoseismic evidence of great surface rupture earthquakes along the Indian Himalaya, *J. Geophys. Res.*, *111*, B03304, doi:10.1029/2004JB003309.

### 1. Introduction

[2] The ongoing collision of India into Eurasia has resulted in three major earthquakes along the Himalayan

front during the past  $\sim 100$  years (Figure 1a) [Seeber and Armbruster, 1981]. From east to west, the sequence includes the 1905 Kangra earthquake ( $M_w \sim 7.7$ ), the 1934 Bihar-Nepal earthquake ( $M_w \sim 8.1$ ), and the 1950 Assam earthquake ( $M_w \sim 8.4$ ) [Pandey and Molnar, 1988; Ambraseys and Bilham, 2000; Ambraseys and Douglas, 2004]. Although none of the earthquakes are reported to have produced primary surface rupture [Seeber and Armbruster, 1981], it has generally been assumed on the basis of isoseismals and location that the earthquakes are the result of slip on the Himalayan Frontal Thrust (HFT). Lack of primary surface rupture during the major historical

<sup>1</sup>Center for Neotectonic Studies, University of Nevada, Reno, Nevada, USA.

<sup>2</sup>Department of Geological Sciences, San Diego State University, San Diego, California, USA.

<sup>3</sup>Wadia Institute of Himalayan Geology, Dehra Dun, India.

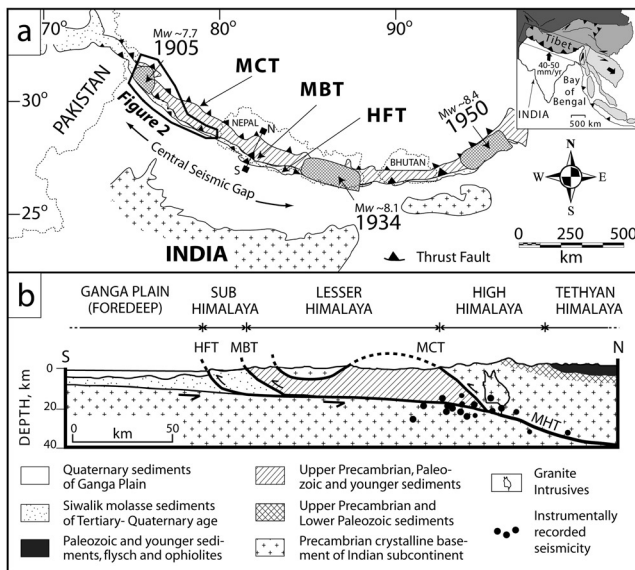


**Figure 1.** (a) Major thrust faults and inferred rupture extents (shaded and labeled with year) of major historical earthquakes along the  $\sim 2500$  km long Himalayan arc. The magnitude and rupture extent of the 1905 Kangra, 1934 Bihar-Nepal, and 1950 Assam earthquakes are from *Pandey and Molnar* [1988]; *Ambraseys and Bilham* [2000]; *Ambraseys and Jackson* [2003]; and *Ambraseys and Douglas* [2004]. The extent of map area shown in Figure 2 is represented as bold polygon in Figure 1a. Three major thrust faults are the Main Central Thrust (MCT), Main Boundary Thrust (MBT), and Himalayan Frontal Thrust (HFT) [Nakata, 1972, 1989]. All the thrust faults are inferred to root at depth in a midcrustal ramp (Main Himalayan Thrust (MHT)) [Zhao et al., 1993; Brown et al., 1996; Nelson and Project INDEPTH Team, 1998]. The area between the rupture bounds of 1905 Kangra earthquake and 1934 Bihar-Nepal earthquake is the Central Seismic Gap of *Khattri* [1987]. The inset shown on the right-hand corner of Figure 1a indicates that ongoing convergence between the Indian and Eurasia is between 40 and 50 mm/yr [De Mets et al., 1994; Paul et al., 2001]. Legend is as in Figure 1b. (b) Generalized north-south geologic section across the Himalaya for the central portion of the Himalayan arc. Instrumental seismicity data are taken from *Ni and Barazangi* [1984]. Location of the cross section in map view is indicated by line connecting solid squares on Figure 1a [Seeber and Armbruster, 1981].

earthquakes has led previous workers to attribute their occurrence to a blind thrust, whereby strain release is expressed as anticline growth rather than primary surface rupture or coseismic surface rupture [Stein and Yeats, 1989; Yeats et al., 1992; Yeats and Thakur, 1998]. In this paper, we describe the late Quaternary expression of the HFT at six sites and demonstrate that the HFT is not blind but, rather, an emergent fault system. We then discuss the mechanical implications that arise if the major historical earthquakes along the HFT have been the result of slip on the HFT but have not produced coseismic surface rupture. Finally, we discuss observations that suggest the HFT has and will produce earthquakes of size greater than those

observed historically, perhaps as large as the greatest thrust earthquakes observed along the major convergent oceanic plate boundaries of the globe.

## 2. Regional Tectonics

[3] The Himalayan mountain belt formed as a result of the collision of India into Eurasia and has accommodated  $\sim 2000$ – $3000$  km of convergence along the  $\sim 2500$  km length of plate boundary since the Eocene (Figure 1a) [Molnar and Tapponnier, 1977]. The collision has produced three major south verging thrust faults that strike the length of the Himalayan arc (Figure 1a). The northernmost is the structurally highest and oldest Main Central Thrust (MCT) system, which dips  $\sim 30^\circ$ – $45^\circ$  northward and marks the contact between the High Himalaya and the Lesser Himalaya (Figures 1a and 1b) [Gansser, 1964]. South of the MCT, the south verging Main Boundary Thrust (MBT) forms a series of north dipping thrust faults that mark the contact between the predominantly pre-Tertiary Lesser Himalayan sediments and the Tertiary and Quaternary sub-Himalayan sediments. The MBT is clearly expressed as a fault in bedrock along nearly its entire length, and in places transports the pre-Tertiary to Quaternary Lesser Himalayan and sub-Himalayan sediments over the younger Quaternary deposits (Figures 1a and 1b) [Nakata, 1972, 1989; Valdiya, 1992]. The southernmost of the three thrusts, and focus of this paper, is the Himalayan Frontal Thrust (HFT), which marks the northern limit of the exposed Indian Plate and displaces Tertiary and Quaternary sediments of the Siwalik Group ( $<0.5$ – $18$  Ma) over modern alluvium of the Indo-Gangetic plain along its length [Nakata, 1972] (Figures 1a and 1b). Locally, the HFT is expressed in young alluvium as relatively short and discontinuous range front scarps that cut Quaternary fluvial terraces and alluvial fans [Nakata, 1972, 1989; Valdiya, 1992; Yeats et al., 1992; Wesnousky et al., 1999; Kumar et al., 2001]. All three east-west striking south verging thrusts appear to merge into a common décollement, the Main Himalayan Thrust (MHT) (Figure 1b) [Seeber and Armbruster, 1981; Zhao et al., 1993; Brown et al., 1996; Nelson and Project INDEPTH Team, 1998].

[4] Plate motion models and GPS measurements indicate that the India-Eurasia convergence continues today at a rate of  $\sim 40$ – $50$  mm/yr (inset in Figure 1a) [De Mets et al., 1994; Paul et al., 2001]. Between  $\sim 10$  and  $20$  mm/yr of the total  $\sim 40$ – $50$  mm/yr is taken up by thrusting along the HFT [Bilham et al., 1997; Wesnousky et al., 1999; Lave and Avouac, 2000; Wang et al., 2001; Kumar et al., 2001]. The major historical earthquakes are suggested to have originated beneath the Higher Himalaya north of the MCT and ruptured the entire basal décollement southward to the HFT [Seeber and Armbruster, 1981]. The above interpretation of southward rupture propagation is consistent with the region of most severe shaking and damage associated with the major historical events shown in Figure 1a, which is generally bounded by the MCT to north and the HFT to south [Seeber and Armbruster, 1981]. It is this latter observation that is cited as the principle evidence that the 1905 Kangra, 1934 Bihar-Nepal, and 1950 Assam earthquakes are the result of slip on the HFT [Pandey

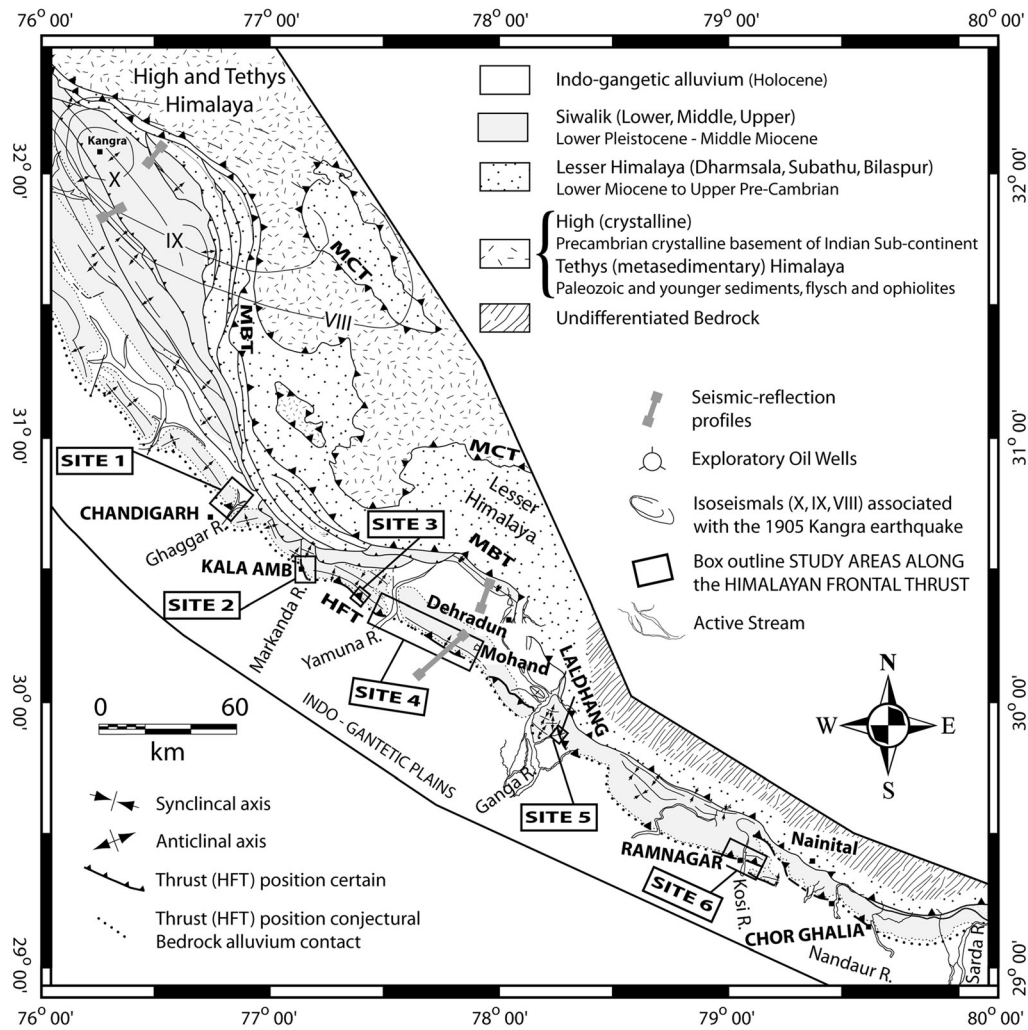


**Figure 2.** Geological map of northwestern portion of the Himalaya (location shown in Figure 1) showing major tectonic features modified and adapted after *Karunakaran and Ranga Rao* [1976] and *Powers et al.* [1998] and from unpublished Oil and Natural Gas Commission (ONGC) maps. Box outlines the approximate area of the Himalayan Frontal Thrust investigated. Active fault traces are adapted and modified after *Nakata* [1972, 1989]; *Valdiya* [1992]; *Wesnousky et al.* [1999]; *Yeats and Lillie* [1991]; and *Yeats et al.* [1992] and those mapped during the present study (see Figure 1 for location).

and *Molnar*, 1988; *Chander*, 1989; *Molnar and Pandey*, 1989; *Ambraseys and Bilham*, 2000].

### 3. Observations

[5] Specific sites discussed in the study (sites 1–6, Figure 2) extend between Chandigarh in the west to Ramnagar in the east along ~250 km stretch of the Indian HFT. We present observations from five new sites together with a previously studied site at Kala Amb (Figure 2). For each site, we use structural, geomorphic, and paleoseismic data to highlight the characteristics of fault displacement along the HFT.

#### 3.1. Chandigarh (Site 1)

[6] Between the longitude  $\sim 76^{\circ}45'$  and  $77^{\circ}00'E$  and near the city of Chandigarh (population  $\sim 800,000$ ), displacement along the northeast to north dipping HFT has pro-

duced an anticline within the Siwalik Group in the hanging wall (site 1, Figures 2 and 3). The anticlinal axis strikes NW from Pinjore Garden with dips of  $\sim 10^{\circ}$ – $70^{\circ}$  SW and  $\sim 20^{\circ}$ – $45^{\circ}$  NE on the southwest and northwest flanks of the anticline (Figure 3). The anticlinal axis takes a sharp southward convex bend near the Ghaggar River with a drastic change in strike and dip in beddings and then changes to a near easterly strike and parallels north of and close to the HFT. The Siwalik beds on the backlimb of the asymmetric south verging anticline southeast of the Ghaggar River show northerly dips ranging between  $\sim 10^{\circ}$  and  $45^{\circ}$  and  $\sim 20^{\circ}$ – $35^{\circ}$  southward on the south limb of the fold structure (Figure 3) [*Sahni and Kahn*, 1964; *Nanda*, 1981].

[7] Fault scarps in Quaternary alluvium are evident along the main trace of the HFT where it cuts and uplifts fluvial terrace deposits along the perennial Ghaggar River (Figures 3 and 4). Five distinct and broad fluvial terrace

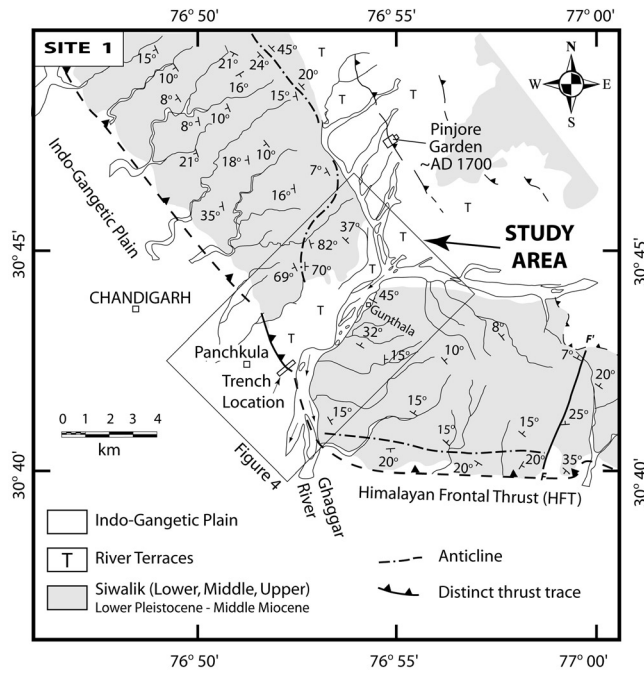


**Figure 3.** Geology of Pinjore Dun area (site 1) adapted and modified after *Sahni and Kahn [1964]* and *Nanda [1981]*. Trench location, major cities (open square), and outline of Figure 4 are also shown (see Figure 2 for location).

surfaces here were first recognized by *Nakata [1972, 1989]* and named, in order of decreasing elevation, the Ghaggar terrace surface (Qt1), Kalka terrace surface (Qt2), Pinjore terrace surface (Qt3), Lower River terrace surface (Qt4) and Modern River terrace surface (Qt5) (Figure 4). Each is truncated by the HFT with the exception of the youngest Qt5 terrace surface. The Modern River terrace surface (Qt5) sits ~14 m above present river grade (Figure 4) and is capped by <1 m of fluvial gravels and overbank deposits which rest unconformably on the northeast dipping Siwalik bedrock and are not cut by the HFT. A radiometric date obtained from undisturbed Qt5 overbank deposits below the active soil provided a modern age (sample JHA-02; Figure 4 and Table 1). The truncation of the Qt2, Qt3, and Qt4 surfaces by the HFT suggests they have been abandoned and preserved primarily as a result of tectonic uplift. The incision of the modern Qt5 terrace by the Ghaggar River, which ranges from ~15 m at Gunthala to ~8 m to the south of the HFT, is most likely attributable to human activity within the drainage basin (Figure 4). The fluvial deposits of Qt4 surface are typically ~12 m in thickness, with the terrace surface and bedrock strath contact at ~32 m and ~20 m above the current stream grade, respectively (Figure 4). Radiocarbon dates of detrital charcoal collected from Qt4 deposits on both sides of the river place a limit on the age of the Qt4 surface. Two fragments of charcoal collected from an undisturbed Qt4 deposits at ~3.3–3.5 m below the Lower River terrace surface (Qt4) near the village of Gunthala on the southeastern margin of the Ghaggar River (samples GAG-03 and GAG-05; Figure 4 and Table 1) yielded ages of A.D. 1284–1401 and A.D. 1216–1383,

respectively. Near the truncation of terrace Qt4 by the HFT, a detrital charcoal sample (sample LRT-01; Figure 4 and Table 1) is collected below the active soil from a pit excavated on the Qt4 surface (Figures 4 and 5). The pit exposed well-rounded, well-sorted fluvial gravels (unit 1) overlain by fine-grained overbank deposits (unit 2) consisting of a fining upward sequence of sand to silty clay deposits with interbedded coarse sand lenses (Figure 5). A silty sand layer containing abundant pottery shards and disseminated charcoal fragments (unit 3) caps the entire exposure. A distinct burnt layer marks the base of unit 3. The charcoal fragment we dated (sample LRT-01) was collected from an undisturbed sedimentary unit (unit 2) at ~1.5 m depth below the present day surface. The age of the sample is A.D. 1036–1207 (sample LRT-01; Figure 5 and Table 1).

[8] The Qt4 terrace sits ~20–32 m above active stream grade while the modern Qt5 surface that is not cut by the HFT sits ~15 m above active stream grade. The ~15 m of incision is historical and probably induced by gravel mining in the upstream reaches of the Ghaggar River, subsequent to the last surface rupture event along the HFT. The age of charcoal (sample JHA-02; Figure 4 and Table 1) extracted from an undisturbed sedimentary bed, places a minimum age on the bedrock surface below the thin fluvial cap. The likelihood of the charcoal arising from recent overbank floods appears slim in light of the ~15 m incision.

[9] Near Gunthala, the bedrock incision of Qt4 and Qt5 terrace surfaces are ~20 and ~14 m, respectively, above

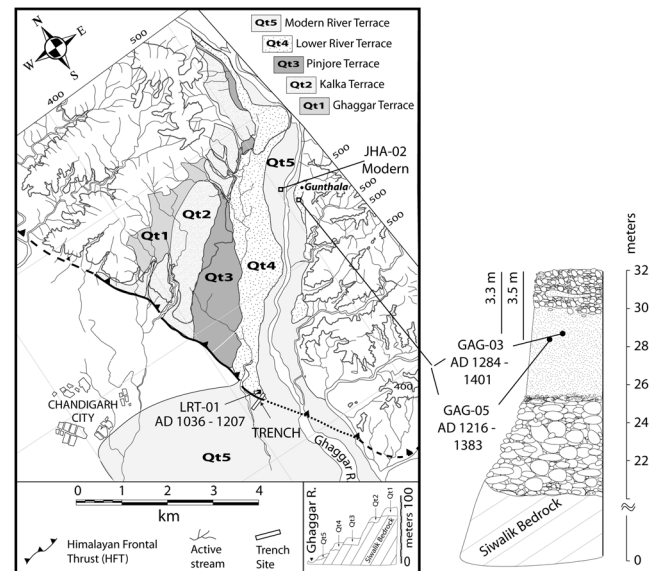


**Figure 4.** (left) Map showing distribution of fluvial terrace deposits along gorge portion of the Ghaggar River, adapted and modified after *Nakata [1972, 1989]*. The location of the trench is shown as long rectangle (not to scale). Contours are at 100 m intervals. A schematic cross profile of terraces is shown in inset at the bottom right corner. (right) Typical character of fluvial terrace deposits resting unconformably over dipping beds of the Siwaliks Group. Heavy black lines show the location of radiocarbon samples (see Figures 2 and 3 for location).

**Table 1.** Radiocarbon Data

Location	Sample	CAMS Number <sup>a</sup>	$\delta^{13}\text{C}^b$	$^{14}\text{C}$ age <sup>c</sup> ( $\pm 2\sigma$ )	Calendar Age Range, <sup>d</sup> Calendar Years B.C. and A.D. ( $\pm 2\sigma$ )
<i>Trench Samples (Site 1)</i>					
Unit 7	PAN-17	94616	-25.0	215 $\pm$ 35	A.D. 1637–1688, 1729–1810, 1922–1949
Unit 7	PAN-11	94615	-25.0	310 $\pm$ 40	A.D. 1482–1654
Unit 7	PAN-09	94614	-25.0	230 $\pm$ 40	A.D. 1522–1576, 1626–1689, 1729–1811, 1922–1949
Unit 6	PAN-03	94612	-25.0	150 $\pm$ 40	A.D. 1665–1784, 1790–1890, 1909–1950
Unit 6	PAN-01	97126	-25.0	535 $\pm$ 35	A.D. 1315–1354, 1387–1441
Unit 6	PAN-02	94611	-25.0	665 $\pm$ 40	A.D. 1279–1330, 1341–1397
Unit 6	PAN-27	94619	-25.0	1250 $\pm$ 40	A.D. 683–884
Unit 4	PAN-23	94617	-25.0	595 $\pm$ 40	A.D. 1299–1413
Unit 4	PAN-26	94618	-25.0	440 $\pm$ 50	A.D. 1404–1523, 1564–1628
Unit 4	PAN-05	97127	-25.0	1115 $\pm$ 35	A.D. 783–789, 827–840, 863–1002, 1011–1016
Unit 4	PAN-08	94613	-25.0	2445 $\pm$ 50	762–678, 671–607, 601–404 B.C.
<i>Terrace and Terrace Pit Samples (Site 1)</i>					
Terrace	JHA-02	94620	-25.0	-855 $\pm$ 45 (?)	post-1950
Terrace	GAG-05	94622	-25.0	735 $\pm$ 40	A.D. 1216–1303, 1368–1383
Terrace	GAG-03	94621	-25.0	645 $\pm$ 45	A.D. 1284–1334, 1336–1401
Pit (unit 2)	LRT-01	97128	-26.0	910 $\pm$ 25	A.D. 1036–1191, 1201–1207
<i>Terrace Samples (Site 2)</i>					
Terrace <sup>c</sup>	MT001-5	77316	-25.0	4300 $\pm$ 40	3015–2878 B.C.
Terrace <sup>c</sup>	MT001-3	73705	-28.4	4410 $\pm$ 40	3325–2915 B.C.
<i>Trench Samples (Site 3)</i>					
Unit 3	AB-08	102806	-25.0	530 $\pm$ 35	A.D. 1319–1352, 1388–1442
Unit 2b <sup>e</sup>	AB-07	102805	-25.0	730 $\pm$ 35	A.D. 1222–1301, 1371–1380
Unit 2b	AB-18	102807	-25.0	1500 $\pm$ 35	A.D. 439–452, 463–518, 529–641
<i>Trench Samples (Site 5)</i>					
Unit 7	LDT-32	97124	-23.7	410 $\pm$ 25	A.D. 1436–1512, 1600–1614
Unit 6	LDT-43	97125	-25.0	470 $\pm$ 70	A.D. 1306–1365, 1386–1527, 1554–1632
Unit 6	LDT-31	97123	-25.2	375 $\pm$ 25	A.D. 1445–1523, 1564–1628
Unit 4	LDT-11	97121	-24.2	660 $\pm$ 35	A.D. 1282–1329, 1343–1395
Unit 3	LDT-15	97122	-24.4	840 $\pm$ 20	A.D. 1163–1174, 1177–1257
Unit 3	LDT-02	97120	-24.6	865 $\pm$ 45	A.D. 1039–1142, 1150–1261
<i>Trench Samples (Site 6)</i>					
Unit 5	BR-07	102802	-25.0	565 $\pm$ 45	A.D. 1301–1371, 1380–1433
Unit 4	BR-06	102801	-25.0	695 $\pm$ 35	A.D. 1278–1323, 1350–1390
Unit 3	BR-15	102804	-25.0	700 $\pm$ 35	A.D. 1259–1322, 1350–1390
Unit 2	BR-09	102803	-25.0	990 $\pm$ 35	A.D. 984–1069, 1080–1129, 1136–1158
<i>Terrace Pit Samples (Site 6)</i>					
Pit (unit 2)	KMRT-03	97129	-26.1	4985 $\pm$ 25	3906–3900, 3894–3881, 3800–3701 B.C.
Pit (unit 2)	KMRT-07	97130	-28.8	6630 $\pm$ 25	5620–5567, 5565–5511, 5498–5485 B.C.

<sup>a</sup>Samples are processed and  $^{14}\text{C}$  measurement are performed at Center for Accelerator Mass Spectrometry (CAMS) at Lawrence Livermore National Laboratory.

<sup>b</sup>The  $\delta^{13}\text{C}$  values are the assumed values according to *Stuiver and Polach* [1977] when given without decimal places. Values measured for the material itself are given with a single decimal place.

<sup>c</sup>Reported  $^{14}\text{C}$  ages use Libby's half-life of 5568 years, relative to A.D. 1950.

<sup>d</sup>Dendrochronologically calibrated age ranges were calculated with the University of Washington calibration program Calib 4.4, using the intercepts method [*Stuiver and Reimer*, 1993; *Stuiver et al.*, 1998], and age ranges are often discontinuous.

<sup>e</sup>Reported radiometric dates are obtained from *Kumar et al.* [2001].

current stream grade. If we assume the difference between the two,  $\sim 6$  m, is the result of uplift due to multiple earthquakes since the abandonment of the terrace surface and bedrock strath (age range of A.D. 1036–1401 obtained from samples GAG-03 (A.D. 1284–1401), GAG-05 (A.D. 1216–1383), and LRT-01 (A.D. 1036–1207); Figure 4 and Table 1), we arrive at a range of maximum bedrock incision rate of  $\sim 4$ – $6$  mm/yr.

[10] We excavated a  $\sim 40$  m long and  $\sim 4$ – $5$  m deep trench (Figure 6) across the fault where it cuts the Lower River terrace surface (Qt4) near the city of Chandigarh (Figures 3 and 4). The trench was located inside the Government College campus in Panchkula, where the fault strikes northwest and is expressed by a  $\sim 2$  m high scarp

(Figures 4 and 6). The northeastern end of the trench exposes four units in the hanging wall (Figure 6). The oldest and lowest (unit 1) is a layer of subrounded, well-sorted, clast supported cobble gravel of fluvial origin. Unit 2 is well sorted, matrix supported fluvial cobble gravels. Unit 3 is subrounded, well-sorted pebble-cobble gravels of fluvial origin. The uppermost and youngest sediments on the hanging wall (unit 4) consist of a thick mantle of extensively bioturbated silty sand overbank deposits. At the crest of the topographic scarp, the flat lying hanging wall units bend abruptly downward and dip  $\sim 12^\circ$  to the southwest. The bend marks the crest of the surface scarp and is associated with two normal faults (F2 and F2') which form a graben and presumably accommodate bending

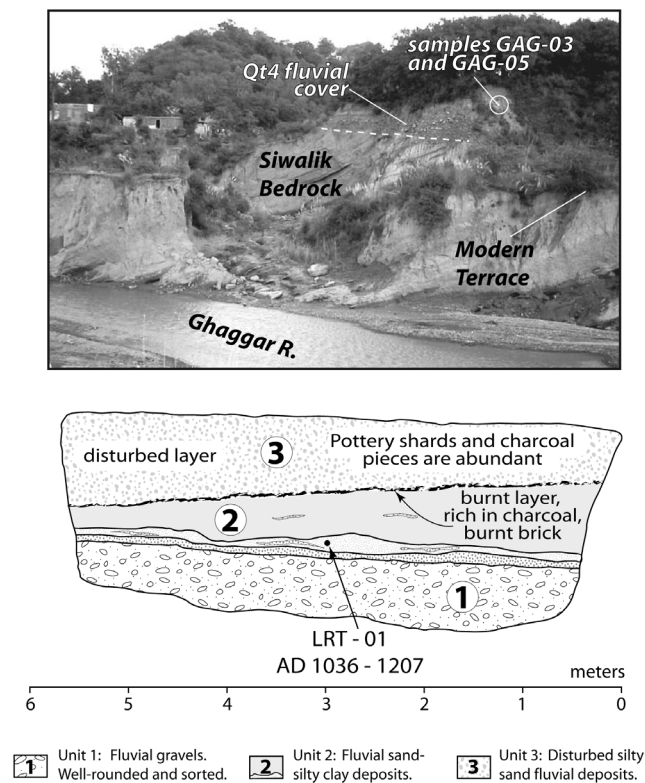


**Figure 5.** (top) Photo of the Lower River terrace (Qt4) deposits preserved along southeastern bank of the Ghaggar River near the village of Gunthala. The contact between the Siwalik bedrock and uplifted fluvial cover is highlighted by white dashed line. The upper gravels preserved on top of the bedrock strath are derived from the Ghaggar River. White open circle denotes the location of radiocarbon samples (see Figure 4 for location). View is toward east. (bottom) Lower River terrace (Qt4) surface sample pit log. The sample pit is located ~100 m to the north of trench location in Figure 4.

associated with folding of the hanging wall. In between faults F2 and F2' and southwestward the hanging wall units dip to form a ramp that parallels the surface expression of the scarp. The southwestern limit of the hanging wall units is marked by a basal thrust fault (F1). The thrust has transported the hanging wall units 1–3 and 4' onto the footwall unit 4. The faulted footwall unit 4 is also observed on the hanging wall. Alternating thin beds of pebbles and fine- to medium-grained sand comprise a cut and fill fluvial channel that caps both the foot and hanging wall units (unit 5). Unit 4' is interpreted to be the basal remnant of unit 4 on the footwall or possibly an older cut and fill deposit analogous to unit 5. Pebble-cobble gravel oriented randomly in a massive silty sand matrix (unit 6) probably represents scarp-derived colluvium. The uppermost and youngest sediments consist of alternating thin beds of fine- to medium-grained silty sand of overbank flood deposits (unit 7).

[11] Radiometrically determined AMS ages of detrital charcoal place limits on the time of displacement registered across the thrust fault F1. Unit 4 is cut by the fault F1. The ages of four detrital charcoal samples collected from unit 4 range in age from 762 B.C. to A.D. 1628 (samples PAN-05, PAN-08, PAN-23, and PAN-26; Figure 6 and Table 1).

Sample PAN-08 is interpreted to be reworked detrital charcoal on the basis of its older age as compared with sample PAN-05 from the same stratigraphic level. Samples PAN-23 and PAN-26 collected near the top of unit 4 are younger in age, A.D. 1299–1413 and A.D. 1404–1628. The stratigraphic inversion of the two dates indicates the samples are reworked detrital charcoal. The correlation of unit 4 across the fault is supported by the overlap in radiocarbon ages of samples taken from the footwall (samples PAN-05, PAN-23, and PAN-26; Figure 6 and Table 1) and hanging wall (samples LRT-01, GAG-03, and GAG-05; Figures 4 and 5 and Table 1) portions of the unit, respectively. That is to say, the ages of PAN-23 and PAN-26 are similar to those found for the Qt4 terrace surface that is cut by the HFT. Taking the youngest age of reworked detrital charcoal as a maximum limiting age of unit 4, the most recent slip on F1 is interpreted to have occurred after A.D. 1404–1628 (sample PAN-26; Figure 6). Units 5 and 6 postdate the displacement on F1. The ages of four samples (samples PAN-01, PAN-02, PAN-03, and PAN-27; Figure 6 and Table 1) collected from the basal portion of colluvial unit 6 range in age from A.D. 683–1950. The range of ages obtained for unit 6 overlap with the ages of PAN-23 and PAN-26 in underlying unit 4. The samples in unit 6 may be reworked from older hanging wall deposits. For these reasons, it is difficult to place a firm upper bound for displacement on the fault, F1. Toward that end, we draw upon a separate observation that Pinjore Garden, located ~10 km to the northeast of the fault, has not incurred any damage from earthquakes since it was built ~A.D. 1600 (Figure 3) [Malik and Nakata, 2003]. On the basis of this observation and coupled with the radiocarbon dates of faulted and unfaulted deposits observed in trench exposure, we suggest that displacement on F1 must be result of an event that occurred after A.D. 1404–1628 (sample PAN-26; Figure 6 and Table 1) but before the Pinjore Garden was built ~A.D. 1600.

[12] A minimum of 2.3 m of slip is recorded in the trench exposure by the thrusting of units 1–3 and 4' over unit 4 (Figure 6). More slip is required to explain the dip panel and apparent vertical separation across the fault. For example, vertical separation across fault strand F1 between the surface at the time of the most recent event, represented by the faulted unit 4, and the present-day hanging wall surface, also unit 4, is 4.4 m (Figure 6). A minimum of 2.3 m slip on fault strand F1 is insufficient to account for the vertical separation (4.4 m) across the fault. Near-surface folding of surficial layers probably accommodates much of the permanent strain at the ground surface.

[13] The surface at the time of the earthquake represented by faulted unit 4 and the uplifted terrace surface of the hanging wall are considered to have been continuous prior to faulting and now exhibit a minimum vertical separation of 4.4 m (Figure 6). If we assume that vertical uplift during the last event accounts for all of the 4.4 m vertical separation, then dividing the vertical separation of 4.4 m across the scarp by the maximum bedrock incision rate of ~4–6 mm/yr determined from the Qt4 terrace implies ~730–1100 years are required accumulate sufficient slip to produce similar size displacements. However, the possibility that a penultimate event also contributed to the scarp height cannot be completely ruled out. The possibility rests

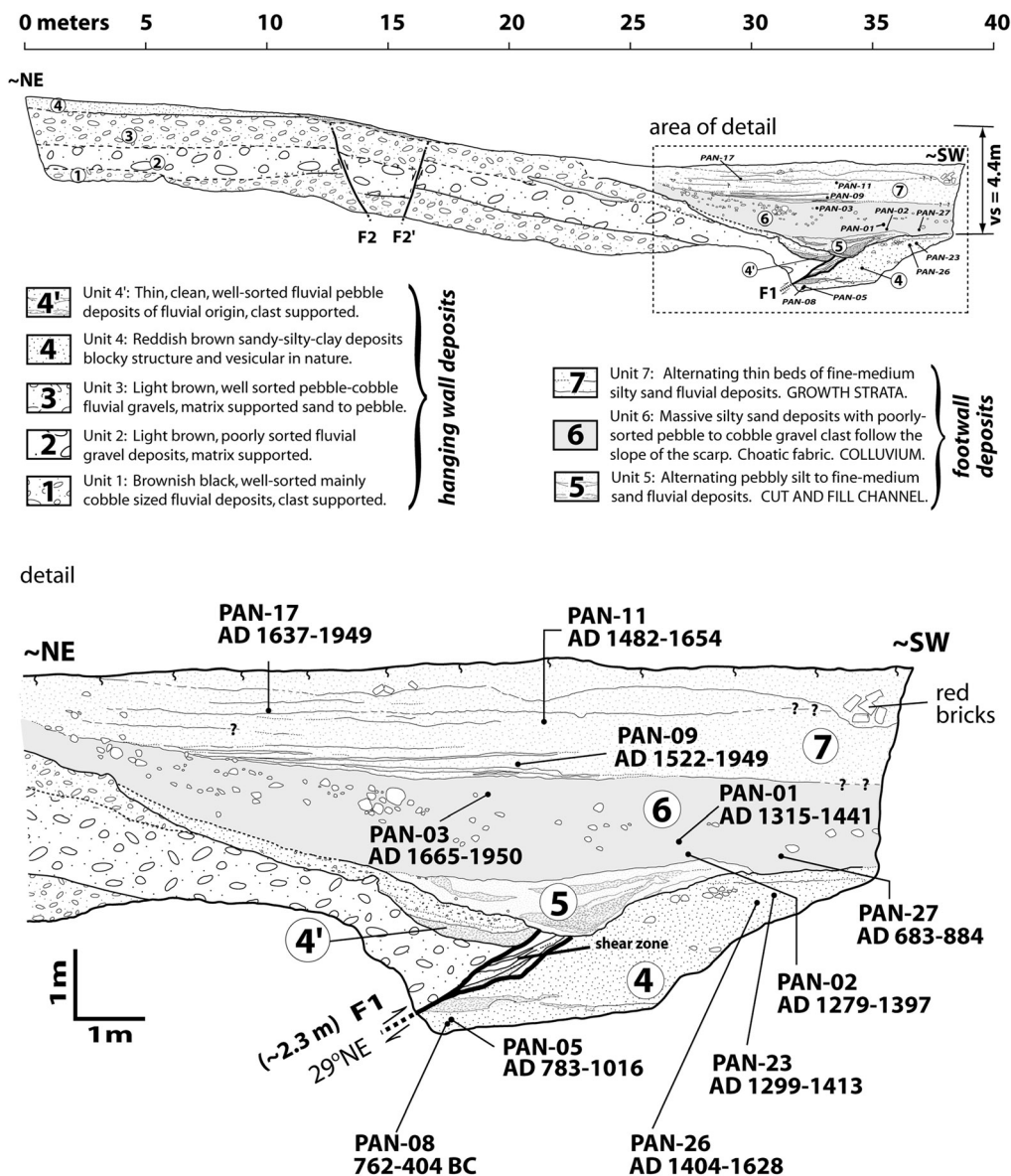


**Figure 6.** Chandigarh trench log (site 1). Outlined in the box is a portion of the trench enlarged to show details of cross-cutting relationship and radiocarbon sample locations (see Figures 3 and 4 for location).

in the presence of unit 4' which may be the remnant of a cut and fill deposit that formed after a penultimate earthquake, analogous to the development of unit 5 subsequent to the most recent displacement. If the scarp was the result of two earthquakes, then the estimated time to accumulate slip to produce similar size displacements would be smaller.

**3.2. Kala Amb (Site 2)**

[14] Kala Amb is located ~40 km to the southeast of Chandigarh and between the longitude ~77°10' and 77°14'E (sites 2 and 3; Figures 2 and 7). The trace of the HFT takes a sharp right step near the town of Kala Amb (Figure 7). The step in the fault trace is a tear fault expressed by a clear scarp in alluvium that truncates and uplifts terraces along the Markanda River (Figure 7) [Kumar et al., 2001]. In contrast, scarps in Quaternary alluvium are not distinct along the main trace of the HFT near Kala Amb.

Displacement on the underlying HFT to the south has produced an asymmetric south verging anticline within the Siwalik Group in the hanging wall (Figure 7). Near Kala Amb, Siwalik beds on the backlimb of the anticline show northerly dips of ~20°–40°. Dip directions reverse and are as steep as ~60° to the south on the forelimb of the anticline [Srivastava et al., 1981].

[15] The Markanda terrace surface sits ~27 m above the present riverbed, of which ~7 m consists of a thick fluvial gravels and relatively thin overbank deposits (Figure 8). Kumar et al. [2001] collected a charcoal sample near the cut bedrock strath below the thick gravel and within primary sedimentary structure which yielded an age range of 3015–2878 B.C. Assuming the age places a minimum bound on the age of the underlying bedrock surface which sits ~20 m above current stream grade, the maximum rate of bedrock incision is calculated to be ~4 mm/yr.

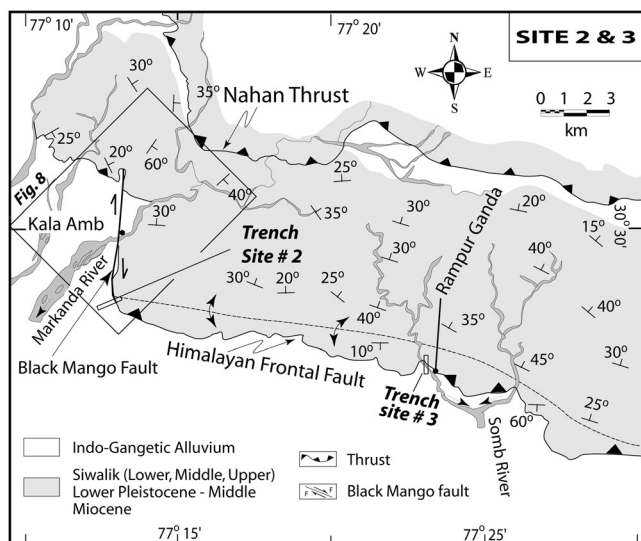


**Figure 7.** Geology of the Kala Amb (site 2) and Rampur Ganda (site 3) area adapted and modified after *Srivastava et al.* [1981]. The location of the trench sites 2 and 3 are shown as a long rectangle (not to scale). Black Mango fault trace near the town of Kala Amb is shown in bold. Arrows on either side of the bold line indicate the probable lateral component of motion. Outline of Figure 8 is also shown (see Figure 2 for location).

[16] *Kumar et al.* [2001] report evidence from a trench exposure of two and possibly three surface rupture earthquakes that have resulted in cumulative coseismic slip of 8.6 m on the tear fault during the last  $\sim 600$  years. The two most recent earthquakes occurred subsequent to A.D. 1294 and A.D. 1423, respectively, and possibly another rupture at  $\sim$ A.D. 260. Minimum displacements during the two most recent earthquakes occurred subsequent to A.D. 1294 and A.D. 1423 were on the order of 5.3–5.4 m and 2.4–4.0 m, respectively, and a possibly larger displacement interpreted for the  $\sim$ A.D. 260 event [*Kumar et al.*, 2001].

### 3.3. Rampur Ganda (Site 3)

[17] The Rampur Ganda study area is located  $\sim 20$  km east of site 2 (Kala Amb), and is labeled site 3 in Figures 2 and 7. Here the trace of the HFT is discontinuously expressed as fault scarps in Quaternary alluvium. We placed a  $\sim 58$  m long trench across an east-west trending scarp near the outlet of the Somb River tributary near the small village of Rampur Ganda (Figure 7). A log of the eastern trench wall is shown in Figure 9. The northernmost hanging wall portion of the trench is composed of two distinctive units (Figure 9). The oldest and lowest (unit 1) is a highly sheared and faulted package of middle Siwaliks sandstone and mudstone. The shear fabric on the Siwaliks increases in intensity toward the south and appears to be the result of repeated tectonic activity. Unit 2a is a well-rounded to subrounded, poorly sorted fluvial sand, cobble and boulder gravel that caps unit 1 along an erosional unconformity. The uppermost and youngest sediment on the hanging wall (unit 2b) is clayey silt to medium sand overbank deposits that shows a weak to moderate soil horization. The unit is  $\sim 2$  m thick to the north and tapers out to only

centimeters in thickness near the inflection of the topographic scarp, after which it disappears entirely because of erosion of the scarp. The flat lying units of the hanging wall bend gradually downward to a maximum dip amount of  $\sim 16^\circ$  to the south. The bend marks the inflection of the surface scarp and is associated with tensional cracks (F4 and F4'), which form a graben and presumably accommodate a portion of the bending (Figure 9). The dipping hanging wall units form a ramp that parallels the surface expression of the scarp. A basal thrust fault (F1) marks the southern limit of the hanging wall. The fault strand F1 has transported the hanging wall units (units 1, 2a, and 2b) over footwall unit 2b'. The lowermost of the footwall units exposed in the trench (unit 2b') consists of dark gray, organic rich clayey silt to medium sand. Unit 2b' is faulted and contains abundant charcoal and pottery shards, and capped by a weak and now buried soil horizon. The unit is interpreted to be the ground surface at the time of the fault displacements on F1, F2, and F3. An unfaulted package of medium to coarse sand with occasional pebbles caps both the foot and hanging wall units (unit 3). Unit 3 is distinguished by thinly (0.5–2 mm) laminated, discontinuous (30–40 cm) sand beds, mostly planar but with occasional fine laminations, which we interpret to be

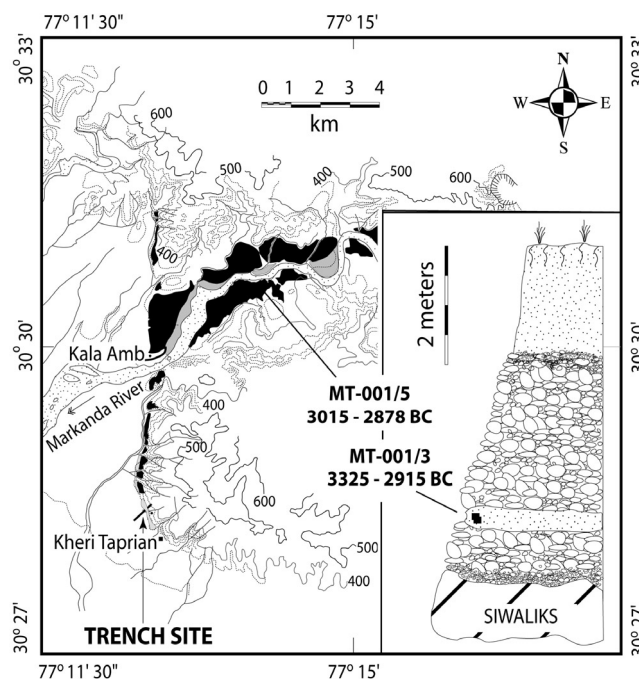


**Figure 8.** Map of fluvial terrace deposits (black shaded polygon) preserved along the Markanda River. Contours of 100 and 20 m intervals are represented as solid and dashed lines, respectively (see Figures 2 and 7 for location). Inset shows typical character of fluvial terrace deposits resting unconformably over dipping beds of the Siwaliks Group. The fluvial terrace deposits are typically composed of rounded pebble-cobble gravels capped by a fine-grained loamy sand unit. Heavy black lines show the location of radiocarbon samples in map view and exposure section. Map is adapted and modified after *Kumar et al.* [2001] (see Figure 7 for location).

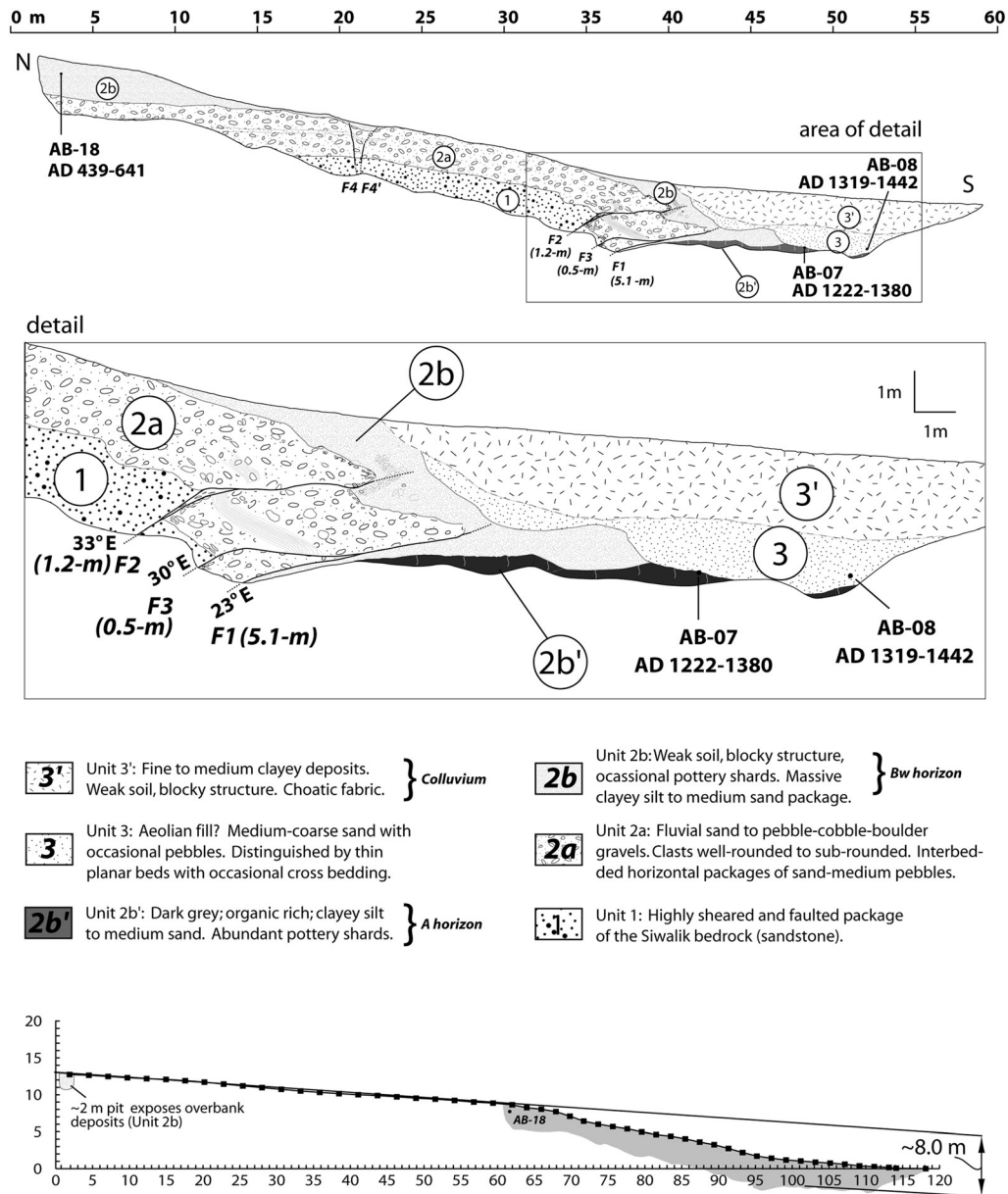


**Figure 9.** (top) Rampur Ganda trench log (site 3). (center) Detail of southern portion of the trench log. (bottom) Scarp profile across the fault trace. The area of actual trench log (top) with respect to scarp profile is represented as gray shaded polygon (see Figure 7 for location).

aeolian accumulation or reworking of moderate to coarse sand at the base of the fault scarp. The uppermost and youngest sediments (unit 3') consist of a fine to medium clayey package with occasional pebble-cobble gravels oriented randomly and are interpreted as scarp-derived colluvium primarily from capping unit 2b on the hanging wall with little to no contribution from fluvial gravel unit 2a along the dip panel.

[18] Fault strand F2 cuts to within a meter from the surface and disrupts the sediments of unit 2b but not the capping units 3 and 3' (Figure 9). Fault strand F3 exhibits minor displacement (~0.5 m) and cuts units 1 and 2a, and transfers slip to and merge with the main strand F1. Fault strand F1 warps and truncates the hanging wall units but not the capping units 3 and 3'. A minimum displacement

of ~5 m along the fault strand F1, measured from the bottom of the trench to the tip of the strand, resulted in warping and sliding of the hanging wall at very low angle and shearing and ploughing of unit 2 and soil horizon (unit 2b'). Shearing and ploughing of sediments was accompanied by brittle displacement along fault strand F1 that transported hanging wall units (units 1, 2a and 2b) over the sheared and bulldozed sediments of units 2 and 2b' now preserved immediately beneath the snout of the upward termination of fault strand F1. Displacement on F1 was followed by aeolian deposition of unit 3 against the fault scarp and emplacement of the scarp-derived colluvium of unit 3'.

[19] Radiometric ages determined for detrital charcoal place limits on the timing of displacement registered across

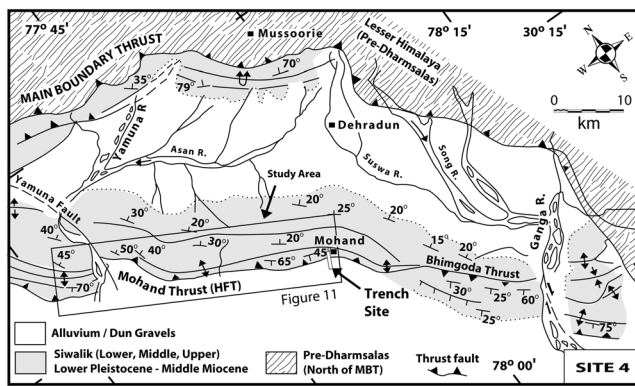


**Figure 10.** Geology of Dehra Dun (site 4) adapted and modified after *Thakur* [1995] and *Wesnousky et al.* [1999]. Location of trench (long rectangle, not to scale) and outline of Figure 11 are also shown. The fault is shown as a solid line where distinct and as a dotted line where inferred (see Figure 2 for location).

the thrust fault strands F1, F2, and F3. A detrital charcoal sample recovered from the youngest faulted soil horizon (unit 2b') limits the most recent fault displacement to after A.D. 1222–1380 (sample AB-07; Figure 9 and Table 1). Sample AB-08 collected from the oldest unfaulted unit 3 limits the most recent earthquake to before A.D. 1319–1442, however, the possibility that sample AB-08 is reworked from the hanging wall unit 2b allows that the most recent earthquake may have occurred after A.D. 1442 (Figure 9 and Table 1). When taken together, radiocarbon dates and fault relations suggest that displacements on the fault traces F1, F2, and F3 occurred during the past ~700 years, between A.D. 1222 and 1442, or later if sample AB-08 is reworked. A detrital charcoal sample (sample AB-18; Figure 9 and Table 1) recovered ~1 m below the surface of unit 2b near the northern end of the trench in the hanging wall provides a radiometric age of A.D. 439–641. The disparity in the ages of radiocarbon samples obtained from unit 2b' (sample AB-07) and unit 2b (sample AB-18) reflects that AB-07 is taken from a paleosol that caps unit 2b, whereas AB-18 is taken from within unit 2b (samples AB-07 and AB-18; Figure 9 and Table 1). The portion of unit 2b that now sits above unit 2b' on the footwall was emplaced tectonically by plowing and displacement at the tip of the fault F1 (Figure 9). The relative lack of erosion of units 2a and 2b on the dip panel and presence of only single colluvial package are interpreted to suggest the scarp is due to a single earthquake displacement and that relatively little time has passed since the scarp was created.

[20] The minimum displacement recorded on strands F1, F2, and F3 in the trench exposure is ~7 m, with 5.1 m, 1.2 m and 0.5 m, respectively (Figure 9). The surface at the time of the earthquake represented by faulted unit 2b' and the uplifted terrace surface of the hanging wall are interpreted to have been continuous prior to faulting and now exhibit a vertical separation of ~8 m. The ~7 m of brittle displacement recorded on fault strands F1, F2, and F3 only explains ~1.5 m of the ~8 m vertical separation across the scarp. The discrepancy in the measurement reflects the minimum nature of the displacement measure-

ments and also that folding and tilting of the hanging wall accommodate a significant portion of the near surface deformation.

### 3.4. Dehra Dun (Site 4)

[21] Displacement along the southernmost north dipping HFT, near Dehra Dun, locally referred to as the Mohand Thrust, has produced a broad south verging anticline within the Siwalik Group in the hanging wall (site 4; Figures 2 and 10) [*Rao et al.*, 1974; *Raiverman et al.*, 1993; *Thakur*, 1995; *Wesnousky et al.*, 1999]. Siwalik beds on the back limb of the anticline show northerly dips ranging between ~20° and 50°. Dip directions reverse and are as steep as ~45°–70° to the south on the forelimb of the anticline [*Thakur*, 1995]. Continuous fault scarps in Quaternary alluvium are not evident along the main trace of the HFT between the town of Mohand and the Yamuna River (Figure 10) [*Nakata*, 1972, 1989]. However, prior drill hole data, seismic reflection profiles [*Rao et al.*, 1974; *Raiverman et al.*, 1993], and short discontinuous fault scarps near the Chapri River and the Tybryon village [*Wesnousky et al.*, 1999] suggest that the fault is emergent near the study area (Figure 11).

[22] The distribution of fluvial terrace deposits previously mapped by *Wesnousky et al.* [1999] is shown in Figure 11. Uplifted and truncated fluvial terrace deposits are present along the ephemeral streams issuing from the sub-Himalayas between the Khajawara and Yamuna Rivers [*Wesnousky et al.*, 1999]. Surveys of the Khajawara and Shajahanpur River terraces show they are not measurably warped or folded where exposed within the ~2 km of the range front. The lack of warping is consistent with the interpretation that the hanging wall undergoes a rigid translation along the underlying HFT. The highest fluvial terrace surfaces at Khajawara and Shajahanpur Rivers are ~30 m above current stream grade, of which ~10 m is a cap of fluvial gravels. *Wesnousky et al.* [1999] collected a radiocarbon sample from a fine grained capping deposit on the Shajahanpur River terrace and obtained an age range of B.C. 1880–1450. With the assumption that the age is a minimum for the age of the underlying bedrock strath surface, we arrive at an estimated maximum bedrock incision rate of ~5–6 mm/yr by dividing the ~20 m incision of Siwalik bedrock below the upper fluvial gravel deposits (~10 m) by the age of the charcoal sample.

[23] We placed a series of trenches within the streambed of Khajawara River and Shajahanpur River. The trenches show that the HFT reaches the surface, covered by only a thin fluvial material sitting on top of the beveled bedrock, in the active streambeds. A representative example of the series of trenches is shown in Figure 12 (Trench ZT-02). The trench is located near the mouth of Khajawara River along the projection of adjacent truncated higher terraces south of the Siwalik range front (Figure 12).

[24] Scarps in young alluvium are not present at the surface along the projection of the fault, and stratigraphic relations in the trench show complete removal of the fault scarps by fluvial processes within the streambeds. The boundary between Siwalik bedrock and alluvial deposits of the floodplain is abrupt and steep. On the basis of the occurrence of Siwalik bedrock overriding young alluvial deposits along a low-angle thrust fault in trench ZT-02, we

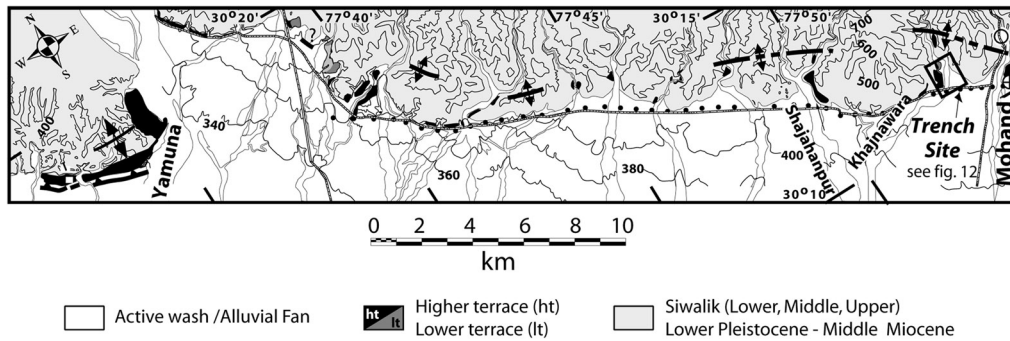


**Figure 11.** Terrace distribution map along the Siwalik range front from near the Yamuna River in the west to the town of Mohand in the east adapted and modified after *Wesnowsky et al.* [1999]. The distinct trace of the Himalayan Frontal Thrust (HFT) is shown as a solid line with teeth on the hanging wall and as a dotted line where inferred. Forest road that runs along the HFT is shown as double lines with hatch. Circle and circle with cross are located at the southeastern end of the map and represent locations of Mohand deep well and nearby shallow exploratory well, respectively. Contours are at 100 m intervals within the bedrock Siwaliks and at 20 m intervals on the alluvial fans. Trench location and outline of Figure 12 are also shown (see Figures 2 and 10 for location).

conclude that repeated earthquakes on an emergent fault have formed the adjacent abrupt and steep escarpments that are characteristic of this section of the range front.

**3.5. Lal Dhang (Site 5)**

[25] Lal Dhang is located ~50 km east of Dehra Dun (site 5; Figure 2). The trace of the HFT is expressed as fault scarps in Quaternary alluvium near the village of Lal Dhang (Figure 13). The Siwalik Hills on the southeastern portion of the map show northeasterly dips generally ranging between 25° and 35° [*Rupke, 1974*]. A trench excavated perpendicular to a northwest trending scarp near the village of Lal Dhang exposed the HFT (Figure 13). The oldest unit exposed by the ~25 m long and ~4–6 m deep trench is an alluvial fan gravel sequence (unit 1), composed mainly of subrounded to rounded cobble to boulder gravel with interbedded lenses of sand (Figure 14). Units 2–5 lie conformably on the fan gravels of unit 1 and extend subhorizontally across the entire base of the trench exposure. Unit 2 is a well-sorted, strongly stratified, and poorly compacted pebble-cobble gravel deposit. Unit 3 consists of alternating layers of poorly compacted sand and silty sand deposits of fluvial origin. Unit 4 is hard, massive silty clay and unit 5 is a thin but distinctive sandy silt deposit characterized by rich organic matter and pottery shards. Units 1–5 are repeated higher in the trench wall, where they are deformed by folding and shearing, and are warped along fault strand F1. Unit 6 is the basal horizon of unfaulted colluvium that consists of poorly laminated massive silty clay. Unit 7, also unfaulted scarp-derived colluvium, is composed of randomly oriented and poorly sorted pebble-cobble gravel in a silty sand matrix and runs nearly the entire length of the trench exposure. A very thin channel deposit is emplaced within the colluvial layer (unit 7a) near the southwestern end of the trench.

[26] Fault strand F1 warps and drags units 1 through 5 on the hanging wall. Unit 6 is not faulted or warped. Thus the top of unit 5 is interpreted to have been the ground surface at the time of displacement along fault strand F1. The hanging wall has slipped at very low angle onto the former

ground surface (unit 5) and bulldozed sediments and soil in front of the lip of the overthrust block. The deformation has resulted in duplication of units 2, 3, and 4 along the front of the thrust. Three detrital charcoal samples were collected and dated from the faulted units 3 and 4. Detrital charcoal

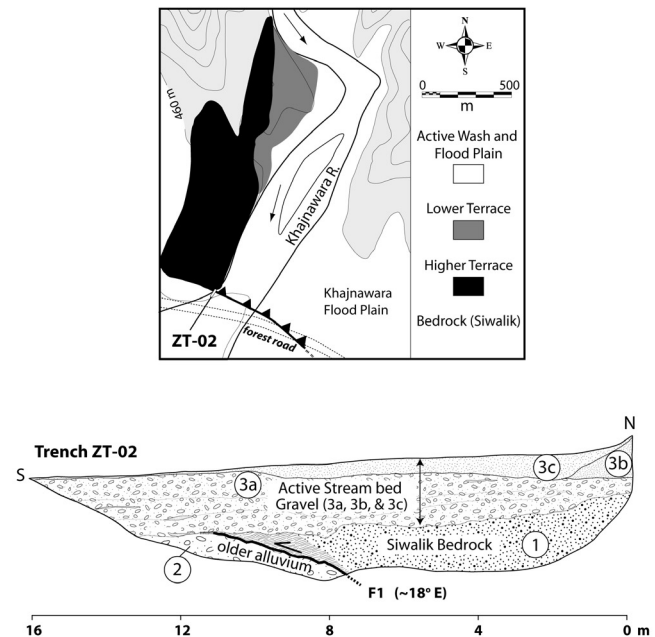


**Figure 12.** (top) Map showing distribution of fluvial terrace deposits preserved along the Khaj nawara River. Higher and lower fluvial terrace deposits are shown as shades of dark and light gray, respectively. Contours are at 20 m intervals. Forest road is shown as dotted lines. The location of trench site is represented as ZT-02. (bottom) Khaj nawara River (Dehra Dun) trench log (site 4). Squiggly line indicates shearing of the bedrock Siwaliks and underlying Quaternary gravel deposits near the fault trace, F1 (see Figures 10 and 11 for location).

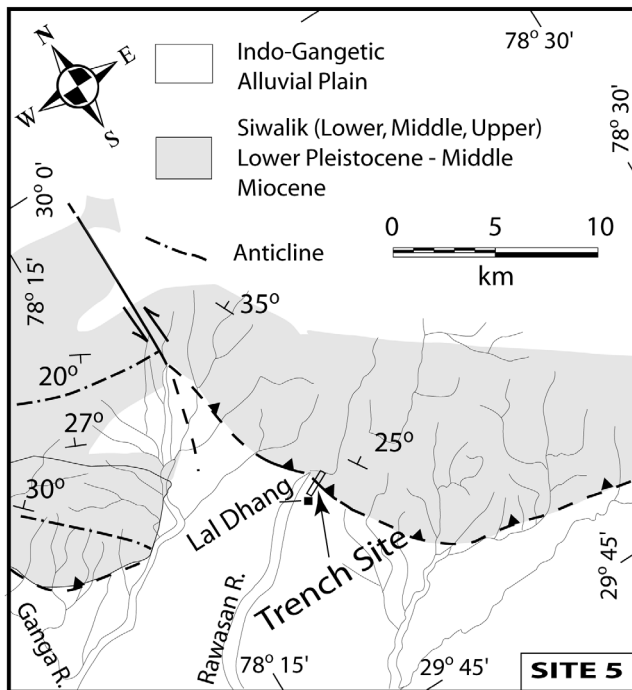


**Figure 13.** Geology of Lal Dhang area (site 5) adapted and modified after *Rupke* [1974]. Fault trace (bold), village of Lal Dhang (solid square) and location of trench site are also shown (see Figure 2 for location).

samples obtained from unit 3 predate the fault displacement and yield dates that range between A.D. 1039 and 1261 (samples LDT-02 and LDT-15; Figure 14 and Table 1). Sample LDT-11, obtained from the faulted unit 4, provides a maximum date of A.D. 1282–1395 for the fault displacement (Figure 14 and Table 1). Two radiometric ages of detrital charcoal samples obtained from the unfaulted unit 6 yield ages between A.D. 1306 and 1632, and are located in deposits that postdate the fault displacement (samples LDT-31 and LDT-43; Figure 14 and Table 1). Taken directly, the radiocarbon ages suggest displacement occurred between A.D. 1282 and 1632. The observation of displaced unit 1 on the foot and hanging walls, the apparently small amount of erosion of the dip panel above the fault, and the small amount and young age of a single package of fault-derived colluvium suggest the entire scarp is due to single earthquake displacement. If samples LDT-31, LDT-32 and LDT-43 collected from unfaulted units 6 and 7 are reworked from hanging wall deposits, one must allow that the event may have occurred after 1632 A.D (Figure 14 and Table 1).

[27] The near horizontal orientation of fault strand F1 and the bulldozing and deformation of sediments indicates proximity to the tip of a thrust. The thrust must steepen at depth to have cut and transported units 1–5. Vertical separation between top of the surveyed hanging wall surface and the surface at the time of faulting (unit 5) in the footwall is a minimum of  $\sim 9.0$  m (Figure 14). Since the fault is subhorizontal, restoration of  $\sim 7$  m (minimum) brittle displacement recorded in the trench on fault strand F1 will yield an insignificant value to explain the vertical separation. The discrepancy in the measurement indicates the possibility that much of the displacement is accommodated

in near-surface folding and tilting, and production of the dip panel that forms the scarp.

### 3.6. Ramnagar (Site 6)

[28] Near Ramnagar (site 6; Figure 2), displacement along the southernmost north dipping HFT has produced a broad south verging anticline within the Siwalik Group (Figure 15) [Rao *et al.*, 1973]. The Siwalik Hills on the western portion of the mapped area comprise mainly homoclinal strata with dips on the northern flank generally ranging from  $\sim 10^\circ$ – $35^\circ$ . Dip directions reverse and are as steep as  $\sim 70^\circ$  to the south on the forelimb of the anticline. To the east of the Kosi River, Siwalik beds take a sharp right step to the south of Dabka River. To the southeast of Dabka River, dip directions on the backlimb of the Siwaliks show northerly dip ranging from  $\sim 10^\circ$  to  $20^\circ$ , whereas the south side of the forelimb of the anticline show dips ranging from  $\sim 30^\circ$  to  $70^\circ$  (Figure 15) [Rao *et al.*, 1973]. Fault scarps in Quaternary alluvium are present along the main trace of the HFT within the mapped area (Figures 15 and 16) [Nakata, 1972]. The HFT is expressed as relatively continuous fault scarp in alluvium between the Swalده and Kosi Rivers. East of the Kosi River, the HFT is discontinuously expressed and takes a right step toward the south along the Siwaliks.

[29] Terraces offset by the HFT along the Kosi River occur on both banks of the Kosi River (Figures 15 and 16) [Nakata, 1972]. All the terrace surfaces are truncated by the east to southeast trending HFT. The oldest surface, Qt1, sits  $\sim 90$  m above the present riverbed, of which  $\sim 25$  m consists of thick fluvial gravels capped by a relatively thin overbank deposit (Figure 16). The intermediate aged fluvial terrace deposits (Qt2) are  $\sim 15$  m thick, with terrace surfaces and bedrock strath contacts at  $\sim 50$  and  $\sim 35$  m above the present riverbed, respectively (Figure 16). The Lower River terraces (Qt3) are  $\sim 14$  m above present river grade and are generally capped by a  $\sim 4$  m cover of fluvial gravels and overbank deposit on the gently dipping Siwalik bedrock strath (Figure 16). Terrace surface, Qt3, occurs along the smaller ephemeral streams that issue from the Siwalik Hills, and a broad remnant of the surface is locally preserved along the Swalده, Chor Pani, and Karkat Rivers.

[30] We excavated a  $\sim 2$  m deep pit on the Qt2 surface a few kilometers north of Ramnagar near the village of Ringcora (Figure 16). The oldest deposits exposed in the pit (Figure 16) are subrounded, well-sorted fluvial gravels (unit 1). The gravels of unit 1 are capped by bioturbated fine-grained overbank deposits of clay to silty sand (unit 2). Radiometric dates of two detrital charcoal fragments (samples KMRT-03 and KMRT-07; Figure 16 and Table 1) collected from unit 2 below the present-day surface limit the age of the terrace surface to 3906–3701 B.C. and 5620–5485 B.C., respectively. Detrital charcoal samples were purposely recovered from near the contact of the fluvial gravel and overlying cap of overbank deposits to avoid sampling of reworked charcoal. Although the location of samples suggests original deposition, the presence of termite mounds and lack of primary sedimentary structures raise concern that the detrital charcoal may have been emplaced subsequent to terrace formation and hence post-dates the abandonment of the bedrock strath. Assuming the samples KMRT-03 (3906–3701 B.C.) and KMRT-07

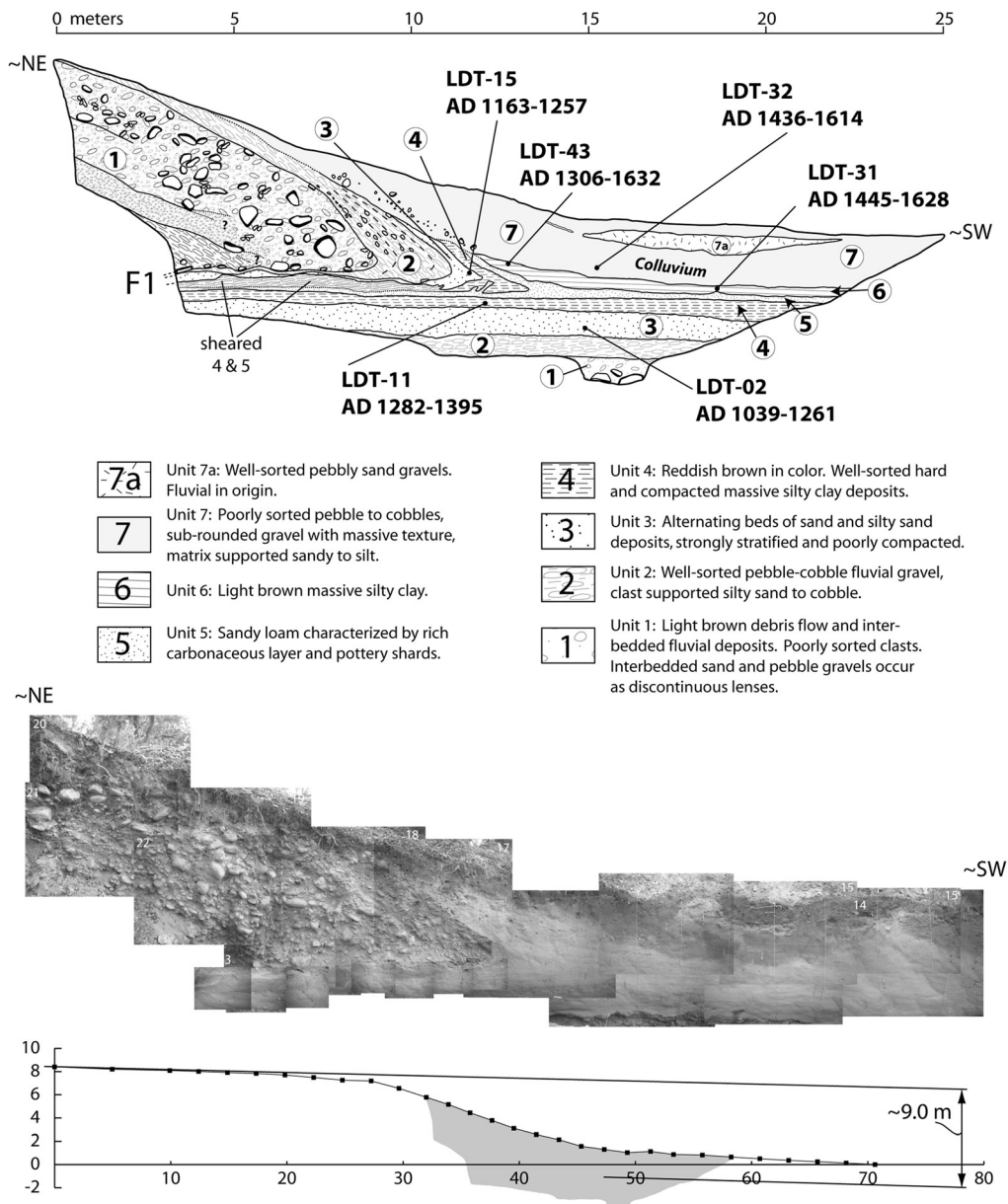


**Figure 14.** (top) Lal Dhang trench log (site 5). (center) Photo mosaic of the trench log shown at top. (bottom) Scarp profile across the fault trace. The area of Lal Dhang trench log (top) is shown with respect to scarp profile as gray shaded polygon (see Figure 13 for location of trench).

(5620–5485 B.C.) ages are close in time to the formation of the Qt2 surface, a range of maximum bedrock incision rate of ~5–6 mm/yr is obtained by dividing the sample age values into the 35 m of bedrock uplift of Qt2 surface above the present stream bed.

[31] We opened a ~32 m long trench perpendicular to the fault where it cuts and truncates the Qt3 terrace deposits near the Karkat River (Figure 16). At this location, the fault strikes east-west and is expressed by a ~13.0 m scarp. A detailed log of the eastern trench wall is provided in Figure 17. Five distinct units exposed (unit 1 through 5) from base to top span the entire length of the trench (Figure 17). The oldest exposed unit at the base of the trench is rounded to well-rounded, poorly stratified sand and medium boulder gravels (unit 1). Unit 2 is a

distinctive, mottled light tan to yellow sandy clay layer. Unit 2 shows a facies change toward the northern end of the trench, where medium to coarse-grained sand to pebble gravel channels can be correlated on opposite walls of the trench and indicate scarp-parallel paleoflow direction. Overlying unit 2 is clayey medium- to coarse-grained sand (unit 3). Occasional discontinuous gravel stringers and increasing clay content toward the top of the unit distinguishes unit 3 from unit 2. Unit 4 is clayey silt to coarse sand distinguished by well-defined thin channels. The top of the unit is oxidized and shows red coloration. The youngest and uppermost unit (unit 5) is a dark clayey sand package. The unit shows weak soil structure and few randomly oriented pebbles and cobbles and is interpreted as scarp-derived colluvium (unit 5). All of the exposed

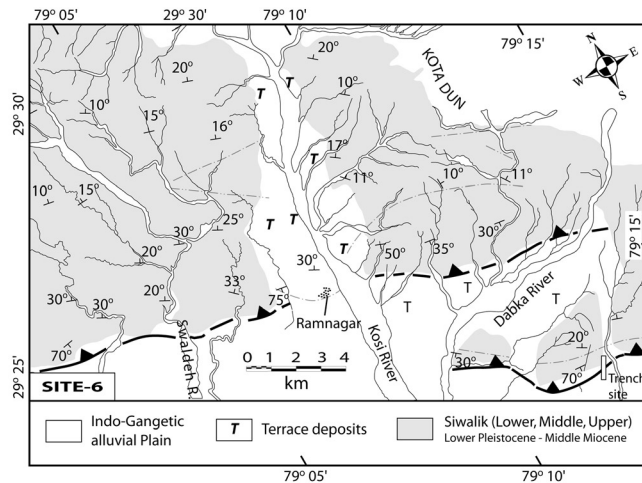


**Figure 15.** Geology of Ramnagar area (site 6) adapted and modified after Rao *et al.* [1973]. The location of the trench is shown as long rectangle (not to scale) on southeastern corner of the map (see Figure 2 for location).

units, with the exception of unit 5, are cut and deformed by thrust fault strands, F1, F2, and F3 (Figure 17). The exposed sediments dip  $\sim 16^\circ$  to the south and parallel the surface expression of the fault scarp.

[32] The northernmost of the fault strands, F3 strand, splays into three slivers that displace and deform units 1–4 (Figure 17). Fault strand F2 displaces and folds all units except unit 5. The southernmost fault strand, F1, also displaces and folds all units but unit 5. Fault strands F1, F2, and F3 record displacements of 1, 1.4, and 1.4 m, respectively (Figure 17).

[33] A detrital charcoal sample obtained from faulted unit 2 predates the fault displacement and is dated at A.D. 984–1158 (sample BR-09; Figure 17 and Table 1). Sample BR-15 collected from the overlying faulted unit 3 provides a radiometric age of A.D. 1259–1390 and sample BR-06 recovered from the youngest faulted package (unit 4) yields an age of A.D. 1278–1390 (samples BR-15 and BR-06; Figure 17 and Table 1). Thus the detrital charcoal sample BR-06 collected from the youngest faulted unit 4 provides a radiometric age that limits faulting to after A.D. 1278–1390. Detrital charcoal (sample BR-07; Figure 17 and Table 1) collected from the unfaulted colluvial package (unit 5) appears to limit the most recent displacement to before A.D. 1301–1433. This upper bound is not firm when considering that it is possible that sample BR-07 may be reworked and hence older than the deposit in which it sits. On these bases, the total brittle displacement of  $\sim 4$  m recorded along fault traces F1, F2, and F3 is interpreted to be the result of one earthquake that occurred  $\sim 700$  years ago, after A.D. 1278 and with less certainty, before A.D. 1433.

[34] The correlation of displaced units 1, 2, 3, and 4 on the foot and hanging walls, the apparently small amount of erosion of the dip panel above the fault, and the small amount and young age of a single episode of fault-derived colluvium suggest the entire scarp is due to single earthquake displacement. The surface at the time of the most recent earthquake, represented by faulted unit 4 in the footwall, and the surface of the present-day terrace on the

hanging wall are separated by at least 13.0 m (Figure 17). Restoration of brittle displacement recorded on fault strands F1, F2, and F3 only explains a small portion of the total  $\sim 13.0$  m vertical separation. The disagreement between the amount of offset observed along visible fault traces and the displacement required to produce  $\sim 13.0$  m of vertical separation suggests that most of the strain is accommodated by tilting and folding of the hanging wall, in addition to fault displacement along F1.

#### 4. Discussion and Conclusions

[35] Displacement along the underlying north dipping HFT has produced an asymmetric south verging anticline within the Siwalik Group in the hanging wall. The structure has been attributed to fault bend or fault propagation folding [Raiverman *et al.*, 1993; Thakur, 1995; Powers *et al.*, 1998]. The folding of Siwalik bedrock north of the HFT and the occurrence of large historical earthquakes that apparently have not broken the surface have been the basis to suggest that the HFT is a blind thrust [Stein and Yeats, 1989; Yeats *et al.*, 1992; Yeats and Thakur, 1998]. Lack of apparent surface expression of the HFT has also led some workers to believe that the HFT is concealed by Quaternary deposits or eroded [Raiverman *et al.*, 1993; Valdiya, 2003]. Our observations gained from shallow trenches excavated at 6 sites along a  $\sim 250$  km section of the Indian Himalaya

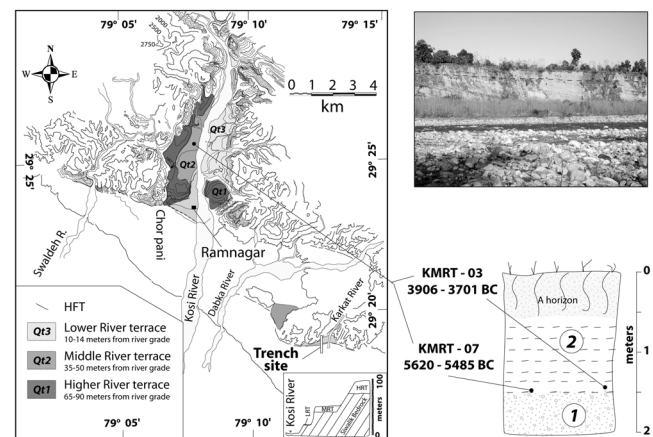


**Figure 16.** (left) Distribution of fluvial terrace deposits along the Kosi River (site 6). Contour intervals are at 50 feet. Location of trench (rectangular box) and radio-carbon samples (solid circle) are also shown. Shown in the inset are profile of the Kosi River terraces and their relation to active river grade. (right) Photo at top shows Middle River terrace (Qt2) deposits sitting unconformably on top of the bedrock Siwaliks. The dashed line indicates the contact between the fluvial terrace deposits and Siwalik bedrock strath. View is to the west. (bottom) A schematic illustration of the sample pit which exposed the upper  $\sim 2$  m of  $\sim 15$  m of fluvial terrace deposits. The exposed fluvial terrace deposits are typically composed of rounded cobble-boulder gravels capped by a fine-grained loamy sand unit. Map locations and context of dendrochronologically corrected ages of samples KMRT-03 and KMRT-07 are shown in map at left and sample pit log, respectively (see Figures 2 and 15 for location).

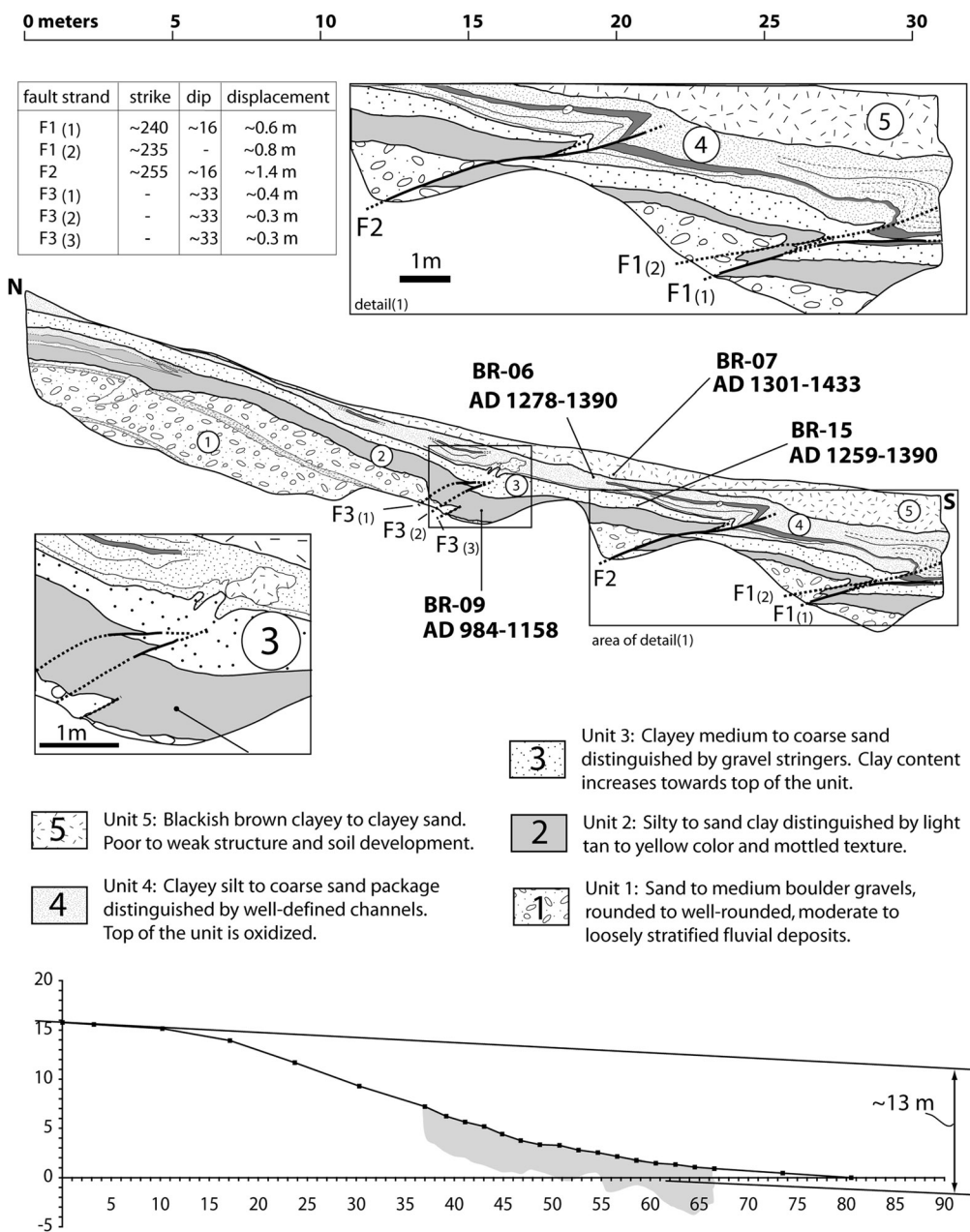


**Figure 17.** (top) Ramnagar trench log (site 6). Boxes are portion of the trench zoomed in to show discrete offsets of individual fault strands. (bottom) Scarp profile across the fault trace. The area of trench log (top) with respect to scarp profile is represented as gray shaded polygon (see Figures 15 and 16 for location).

demonstrate that the HFT is commonly emergent and breaks young surficial deposits. The surface faulting we observe in the trenches and morphology is on strike with the abrupt and steep contact between the Siwalik range front and alluvial sediments of the Indo-Gangetic plain. In that regard, the abrupt front of the Siwaliks appears to closely mark an emergent fault contact along the entire Indian Himalaya.

[36] Displacement on the HFT has resulted in the occurrence of truncated and uplifted fluvial terrace deposits of varying height and age near the mouths of the Ghaggar, Markanda, Shajahanpur, and Kosi Rivers (Figures 4, 8, 11, and 16). The terraces are characterized by fluvial deposits

sitting on incised bedrock straths. The bedrock incision provides a measure of the long-term rate of uplift because of repeated earthquake displacements. Maximum long-term bedrock incision rates obtained by dividing the elevation of the basal contact of the bedrock strath above modern river grade by the ages of radiocarbon samples obtained from the capping fluvial terrace deposits at the respective sites (Figures 4, 8, 11, and 16) yield rates that range from ~4–6 mm/yr. Estimates of the dip of the HFT based on seismic profiles, deep bore holes, balanced cross sections and structural data within the folded Siwalik Group range from about 20° to 45° [Rao *et al.*, 1974; Lyon-Caen and

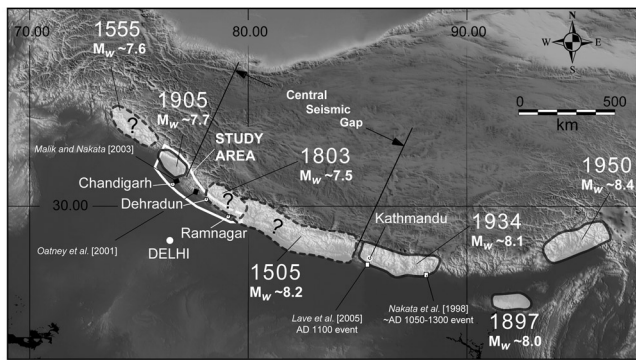


**Figure 18.** Magnitude and rupture extent (shaded) of the 1505, 1555, 1803, 1905, 1934, and 1950 earthquakes (adapted from *Ambraseys and Jackson* [2003], *Ambraseys and Douglas* [2004], and *Bilham and Ambraseys* [2005]). Dashed lines bounding rupture areas of older events emphasize greater uncertainty of bounds because of fewer available historical observations. The area between the rupture bounds of the 1905 Kangra earthquake and 1934 Bihar-Nepal earthquake is central seismic gap of *Khattri* [1987]. Small white circles indicate the study sites (sites 1, 4, and 6). White squares along the southern border of the 1934 Bihar-Nepal earthquake represent paleoseismic sites that report an  $\sim$ A.D. 1100 earthquake that perhaps ruptured 250 km or more [*Nakata et al.*, 1998; *Upreti et al.*, 2000; *Lave et al.*, 2005]. Area of Figure 2 is shown as white polygon. Other paleoseismic trenches within area of Figure 2 are also shown as black squares [*Malik and Nakata*, 2003; *Oatney et al.*, 2001]. No event ages are reported from these trenches.

*Molnar*, 1985; *Schelling and Arita*, 1991; *Raiverman et al.*, 1993; *Srivastava and Mitra*, 1994; *Powers et al.*, 1998; *Kumar et al.*, 2001; *Husson et al.*, 2004; *Lave et al.*, 2005]. The 4–6 mm/yr rates are equivalent to fault slip rates of  $\sim$ 6–18 mm/yr or shortening rates of  $\sim$ 4–16 mm/yr at the respective study sites when uplift is assumed to be the result of slip on an underlying thrust plane dipping between  $20^\circ$  and  $45^\circ$ .

[37] The aerial extent of rupture of large to great historical earthquakes along the  $\sim$ 2500 km long Himalayan arc inferred by others from historical records and the locations of prior trench studies in Nepal are depicted in Figure 18. The observations provide a context with which to view the results of our paleoearthquake studies. Our study area is bounded by the rupture areas estimated for the 1505 Central Himalayan and 1555 Kashmir earthquakes to the east and west, respectively. The larger and more precisely dated 1505 Central Himalayan rupture occurred within the central Himalayan gap of *Khattri* [1987] which he defined to be the region between the 1905 Kangra and 1934 Bihar-Nepal earthquakes (Figures 1, 18, and 19). A  $\sim$ 500–600 km long rupture and a magnitude of  $M_w \sim 8.2$  has been estimated for the 1505 earthquake based on intensity reports from Tibet and India (Figures 18 and 19) [*Ambraseys and Jackson*, 2003; *Ambraseys and Douglas*, 2004]. It has also been proposed that the 1505 rupture area may have filled the entire central seismic gap [*Bilham and Ambraseys*, 2005]. A magnitude of  $M_w \sim 7.6$  is reported for the 1555 Kashmir

event based on the limited intensity reports [*Ambraseys and Douglas*, 2004]. Detailed historical reports are few and the rupture extent shown in Figure 18 for the 1555 earthquake is speculative [*Ambraseys and Jackson*, 2003]. The 1 September  $M_w \sim 7.5$  1803 Kumaon-Garhwal earthquake is inferred to have ruptured  $\sim$ 200 km based on sparse damage reports [*Ambraseys and Jackson*, 2003; *Ambraseys and Douglas*, 2004]. It has been suggested that the 1803 event probably did not produce ground rupture based on the similarity in the aerial extent of strong ground shaking with the 1905 Kangra earthquake which did not produce surface rupture [*Ambraseys and Bilham*, 2000]. Paleoseismic studies in trenches located in central and eastern Nepal allow for an A.D. 1100 event with a rupture length of 250 km or greater (Figure 18) [*Nakata et al.*, 1998; *Upreti et al.*, 2000; *Lave et al.*, 2005].

[38] We present the limits of our radiocarbon dating for the time of displacement at each trench site in a space-time diagram in Figure 19 (bottom). The locations of our study sites are annotated in Figure 19 (top) and along the horizontal axes of the space-time diagram. The horizontal axis is distance in kilometers and is same for both the map and space-time diagram. The vertical axis for the space-time diagram is time in years A.D. The vertical bars within the space-time diagram and above each study site reflect the bounds in age of surface displacements at each site allowed by radiocarbon dates. The lower bounding age of the most recent displacement at all the trenches is firmly constrained by radiocarbon ages obtained from within the faulted units at each of the sites. Radiocarbon ages from within unfaulted units at each site also provide an upper bound on the age of displacement at each site. A strict interpretation of the radiocarbon ages leads to an allowable interpretation that the most recent event in each trench was the result of a throughgoing earthquake between A.D. 1404 and 1422, the range of ages for which limiting ages overlap (Figure 19). However, the resolution is likely only apparent. Reworked carbon is evident in several of the trench sites and the number of radiocarbon ages in unbroken capping deposits at the trench sites (sites 1, 3, 5, and 6) is currently insufficient to rule out that the detrital charcoal is reworked and hence older than the deposit from which it was sampled. In this regard, the upper limiting age on the timing of the most recent displacement at each site may well be younger than suggested by the radiocarbon ages.

[39] The uncertainty in the upper limit on the age of displacement at the trench sites at this time precludes firm correlation to events of the historical record. Considering the large size of displacements observed at Rampur Ganda, Lal Dhang and Ramnagar, it is within reason to suggest that the most recent displacement at each of our study sites occurred simultaneously during a single event. The 1505 event is a possible candidate, although there are at this time no confirming historical reports of large shaking commensurate for such an event in the area at this time. The apparent lack of reported surface ruptures for the more recent and apparently smaller 1803 and 1905 earthquakes also do not appear to be candidates for correlation. As well, it is possible the displacements observed in the trenches reflect an earthquake not yet recognized in the historical record.

[40] Another scenario arises when it is recognized that only at Kala Amb (site 2) do we observe possible evidence

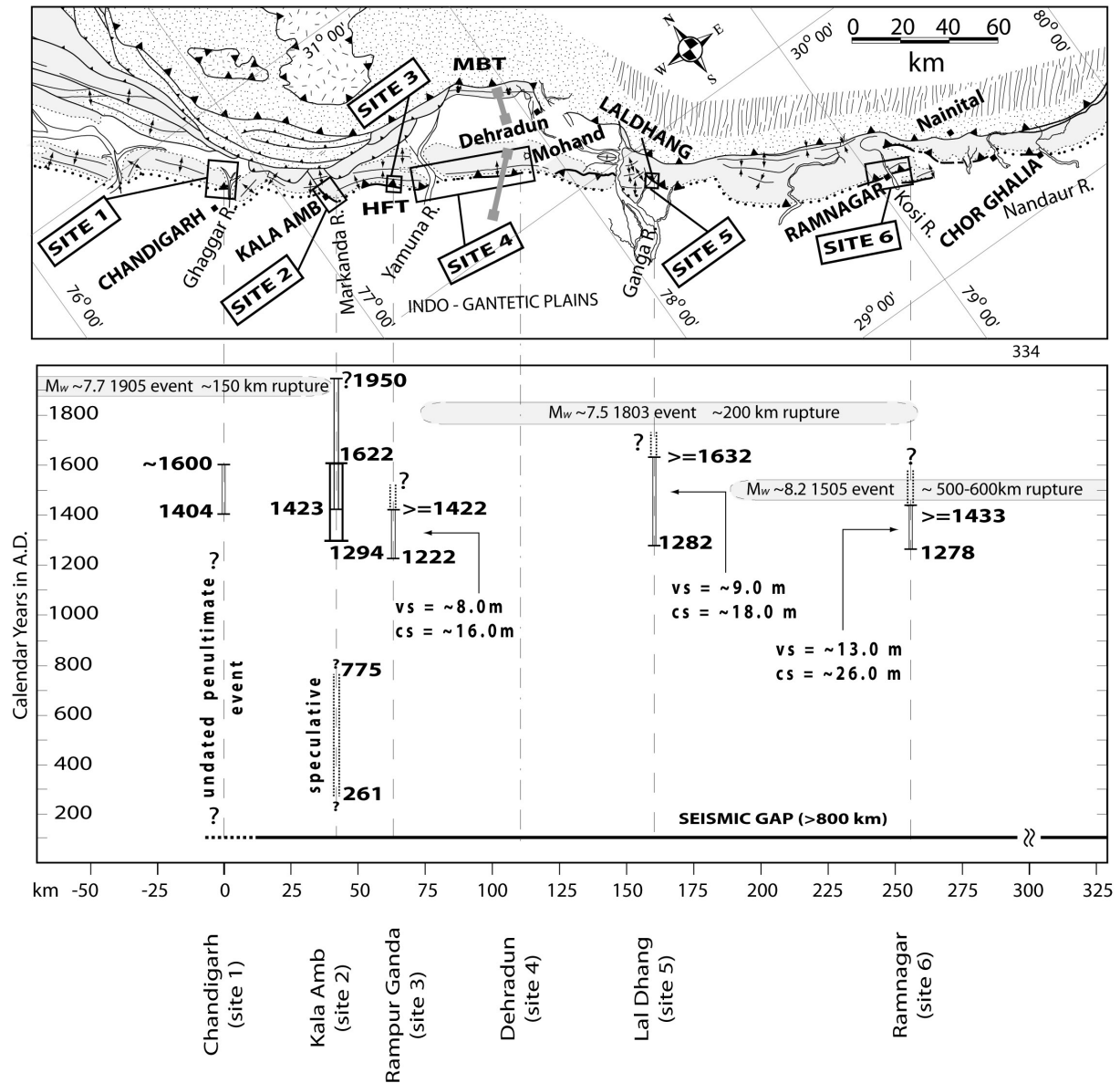


**Figure 19.** (top) Geologic map adapted and modified after Karunakaran and Ranga Rao [1976], Powers et al. [1998], and unpublished Oil and Natural Gas Commission (ONGC) maps. (bottom) Space-time diagram showing radiocarbon constraints on timing of surface displacements at sites 1 through 6. Vertical axis is time in calendar years A.D. and horizontal axis is kilometers. Location of each site is annotated below horizontal axes and overlying geologic map. Horizontal scale of map and space-time diagram is the same. The vertical bars above each study site reflects the time range of surface displacements allowed by radiocarbon dates for the respective locations in calendar years A.D. The coseismic slip (cs) and vertical separation (vs) of the corresponding earthquake is shown in meters. The height of each bar is bounded by 2-sigma standard deviation of the  $^{14}\text{C}$  calendar ages. Solid bold line represents the extent of central seismic gap (>800 km) defined by Khattri [1987]. The rupture extent of known large to great earthquakes within the study area is provided as a long shaded box with magnitude, event age, and inferred rupture length based on Medvedev-Sponheuer-Karnik (MSK) intensity [Ambraseys and Jackson, 2003; Ambraseys and Douglas, 2004; Bilham and Ambraseys, 2005].

of two paleoseismic displacements. Additionally, the coseismic displacements at Kala Amb and Chandigarh (sites 1 and 2) appear to be less than the offsets interpreted to the east at sites 3, 5, and 6. These observations and radiocarbon ages

allow speculation that Kala Amb is a zone of two abutting but slightly overlapping ruptures of different age. In this case, it would be plausible that trench sites 3, 5, and 6 record an event separate from that recorded at site 1. The

possibility would remain that displacements east of Kala Amb (site 2) are related to the 1505 earthquake. The possibility of moving these scenarios from speculation to fact resides in the potential to increase the number and density of radiocarbon ages in the younger capping deposits that are not broken in each trench.

[41] Scarp profiles and trench relations suggest single-event displacements produced vertical separations of  $\sim 8.0$ ,  $9.0$ , and  $13$  m at Rampur Ganda, Lal Dhang, and Ramnagar (Figures 9, 14, 17). The trench exposures at each site show shallow fault strands that generally dip less than  $30^\circ$ , with values ranging between  $0^\circ$  and  $33^\circ$ . The folding observed in the hanging wall at each site requires that the fault dip observed in the trenches increase somewhat at depth. Firm control on the dip of the shallow HFT only exists at Mohand where a  $30^\circ$  dip is confirmed by a deep bore hole and shallow exploratory well [Rao et al., 1974; Lyon-Caen and Molnar, 1985; Raiverman et al., 1993]. An assumption of a  $30^\circ$  dip is consistent with Andersonian mechanics [Anderson, 1951] for thrust faults. Values ranging from  $20^\circ$  to  $45^\circ$  have been suggested by others based on seismic profiles, deep bore holes, balanced cross sections and structural data within the folded Siwalik Group [Rao et al., 1974; Lyon-Caen and Molnar, 1985; Schelling and Arita, 1991; Raiverman et al., 1993; Srivastava and Mitra, 1994; Powers et al., 1998; Kumar et al., 2001; Husson et al., 2004; Lave et al., 2005]. Taking values of  $20^\circ$  and  $45^\circ$  as maximum bounding values on the dip of the HFT at shallow depths and  $30^\circ$  as a preferred value, single-event fault displacements of  $\sim 16 +7/-5$ ,  $18 +8/-5$ , and  $26 +12/-8$  m are required to explain the vertical separations observed at Rampur Ganda, Lal Dhang, and Ramnagar, respectively. The values are comparable to the average dip-slip displacement of  $\sim 12$  m,  $\sim 19$  m and  $\sim 20$  m calculated for the large plate boundary events such as the 1964 Southern Alaska earthquake ( $M_w$  9.2), the 1960 Southern Chile earthquake ( $M_w$  9.5), and the 2004 Indonesia/Andaman earthquake ( $M_w$  9.0), respectively [Sykes and Quittmeyer, 1981; Park et al., 2005]. Each of these events was characterized by rupture lengths of  $\sim 750$ ,  $1000$ , and  $1300$  km, respectively, whereas our observations extend only to the western end of the inferred  $\sim 500$ – $600$  km rupture of 1505 earthquake along the Indian HFT. The observations are consistent with the idea of simultaneous rupture of these sites in a single great earthquake, and perhaps, during 1505.

[42] An estimate of the time required to accumulate sufficient slip to produce similar size displacements to those we observe is obtained by dividing the vertical separation due to estimated single-event displacements by the longer term uplift rate determined from estimates of the rate of incision of bedrock underlying uplifted fluvial terrace deposits. To do so, we divide the vertical separation measurements of  $\sim 8.0$ ,  $\sim 9.0$ , and  $\sim 13.0$  m obtained for Rampur Ganda, Lal Dhang and Ramnagar by the average long-term bedrock incision rates of  $\sim 4$ – $6$  mm/yr obtained from uplifted terraces at the Ghaggar, Markanda, Shajahanpur, and Kosi Rivers. The exercise yields estimates of  $\sim 1330$ – $2000$ ,  $\sim 1500$ – $2250$ , and  $\sim 2170$ – $3250$  years or more for sufficient slip to accumulate to produce the observed coseismic slips, respectively.

[43] Instrumentally recorded seismicity of moderate magnitude seismic events is concentrated beneath the High

Himalaya (Figure 1) [Ni and Barazangi, 1984], and geodetic monitoring also shows that interseismic elastic strain accumulation is presently localized beneath the High Himalaya [Bilham et al., 1997; Jackson and Bilham, 1994; Pandey et al., 1995; Banerjee and Burgmann, 2002]. When combined with evidence of an emergent HFT, these observations are consistent with the interpretation that the major historical earthquakes initiated at a point of localized strain accumulation beneath the MCT and propagated southward as much as  $100$  km along a shallow décollement that surfaces as the HFT [Pandey et al., 1995; Brune, 1996; Bilham et al., 1998; Lave and Avouac, 2000].

[44] The 1905, 1934 and 1950 events that occurred in last century along the HFT apparently have not produced coseismic surface ruptures (Figures 1 and 18). Given our observations showing evidence of surface rupturing earthquakes, the question arises why surface rupture has not been recorded for the 1905, 1934, and 1950 events. It seems unlikely but possible that studies of these major historical earthquakes missed evidence of surface rupture. If the historical earthquakes did not rupture the surface, how are we to interpret the surface ruptures that we do observe? We suggest on the basis of size and possible synchronicity of displacements recorded in the trenches that there exists the potential for earthquakes yet larger than recorded in the historical record capable of producing surface rupture lengths greater than the  $\sim 250$  km we have studied along the HFT.

[45] **Acknowledgments.** We thank Usha Malik (Principal) of Government College, Panchkula, and Dhanpat Singh, Higher Education Commissioner, Government of Haryana, for allowing us to place trenches inside the campus of Government College, Panchkula. We thank forest officials of Uttaranchal Government for showing interest and support for the project by providing us permission to dig trenches and sample pits in the Reserved and National Forest areas of the Uttaranchal region. The support and interest shown by scientists at Wadia Institute of Himalayan Geology, Dehra Dun, is greatly appreciated. We thank Jérôme Lave, Robert Yeats, and Associate Editor Isabelle Manighetti for their thorough and thoughtful comments. Finally, we thank Sanjay Verma for driving and helping us in the field. This material is based upon work supported by National Science Foundation grant EAR9972955 and in part by a Graduate Student Association Grant, University of Nevada, Reno. This is Center for Neotectonic Studies contribution 45.

## References

- Ambraseys, N., and R. Bilham (2000), A note on the Kangra  $M_s = 7.8$  earthquake of 4 April 1905, *Curr. Sci.*, *79*, 45–50.
- Ambraseys, N., and J. Douglas (2004), Magnitude calibration of north Indian earthquakes, *Geophys. J. Int.*, *159*, 165–206.
- Ambraseys, N., and D. Jackson (2003), A note on early earthquakes in northern India and southern Tibet, *Curr. Sci.*, *84*, 571–582.
- Anderson, E. M. (1951), *The Dynamics of Faulting*, 206 pp., Oliver and Boyd, White Plains, N. Y.
- Banerjee, P., and R. Burgmann (2002), Convergence across the northwest Himalaya from GPS measurements, *Geophys. Res. Lett.*, *29*(13), 1652, doi:10.1029/2002GL015184.
- Bilham, R., and N. Ambraseys (2005), Apparent Himalayan slip deficit from the summation of seismic moments for Himalayan earthquakes, 1500–2000, *Curr. Sci.*, *88*, 1658–1663.
- Bilham, R., et al. (1997), GPS measurements of present day convergence across the Nepal Himalaya, *Nature*, *386*, 61–64.
- Bilham, R., et al. (1998), Geodetic constraints on the translation and deformation of India, implications for future great Himalayan earthquakes, *Curr. Sci.*, *74*, 213–229.
- Brown, L. D., et al. (1996), Bright spots, structure, and magmatism in southern Tibet from INDEPTH seismic reflection profiling, *Science*, *274*, 1688–1691.
- Brune, J. N. (1996), Particle motions in a physical model of shallow angle thrust faulting, *Proc. Indian Acad. Sci. Earth Planet. Sci.*, *105*, L197–L206.

- Chander, R. (1989), Southern limits of major earthquake ruptures along the Himalaya between 15 deg. E and 90 deg. E, *Tectonophysics*, *170*, 115–123.
- De Mets, C., et al. (1994), Effect of recent revisions to the geomagnetic reversal time scale on estimates of current plate motions, *Geophys. Res. Lett.*, *21*, 2191–2194.
- Gansser, A. (1964), *Geology of the Himalayas*, 289 pp., Wiley Interscience, Hoboken, N. J.
- Husson, L., et al. (2004), Kinematics and sedimentary balance of the Sub Himalayan zone, western Nepal, in *Thrust Tectonics and Hydrocarbon Systems*, edited by K. R. McClay, *AAPG Mem.*, *82*, 115–130.
- Jackson, M. E., and R. Bilham (1994), 1991–1992 GPS measurements across the Nepal Himalaya, *Geophys. Res. Lett.*, *21*, 1169–1172.
- Karunakaran, C., and A. Ranga Rao (1976), Status of exploration for hydrocarbons in the Himalayan region, in *Contributions to Stratigraphy and Structure, Himalayan Geology Seminar, Section III, Oil and Natural Gas Resources*, *Geol. Surv. India Misc. Publ.*, *41*, 1–66.
- Khattri, K. N. (1987), Great earthquakes, seismicity gaps and potential for earthquake disaster along the Himalaya plate boundary, *Tectonophysics*, *138*, 79–92.
- Kumar, S., et al. (2001), Earthquake recurrence and rupture dynamics of Himalayan frontal thrust, India, *Science*, *294*, 2328–2331.
- Lave, J., and J. P. Avouac (2000), Active folding of fluvial terraces across the Siwaliks Hills, Himalayas of central Nepal, *J. Geophys. Res.*, *105*, 5735–5770.
- Lave, J., et al. (2005), Evidence for a great Medieval earthquake (~1100 A.D.) in the central Himalayas, Nepal, *Science*, *307*, 1302–1305.
- Lyon-Caen, H., and P. Molnar (1985), Gravity anomalies, flexure of the Indian Plate, and the structure, support and evolution of the Himalaya and Ganga basin, *Tectonics*, *4*, 513–538.
- Malik, J. N., and T. Nakata (2003), Active faults and related late Quaternary deformation along the northwestern Himalayan Frontal Zone, India, *Ann. Geophys.*, *46*, 917–936.
- Molnar, P., and M. R. Pandey (1989), Rupture zones of great earthquakes in the Himalaya region, *Earth Planet. Sci.*, *98*, 61–70.
- Molnar, P., and P. Tapponnier (1977), The collision between India and Eurasia, *Sci. Am.*, *236*(4), 30–41.
- Nakata, T. (1972), Geomorphic history and crustal movements of the foothills of the Himalayas, *Sci. Rep. Tohoku Univ., Ser. 7*, *22*, 39–177.
- Nakata, T. (1989), Active faults of the Himalaya of India and Nepal, in *Tectonics of the Western Himalayas*, edited by L. L. Malinconico Jr. and R. J. Lillie, pp. 243–264, Geol. Soc. of Am., Boulder, Colo.
- Nakata, T., et al. (1998), First successful paleoseismic trench study on active faults in the Himalaya (abstract), *Eos Trans. AGU*, *79*(45), Fall Meet. Suppl., F615.
- Nanda, A. C. (1981), Occurrence of the Pre-Pinjar beds in the vicinity of Chandigarh, in *GSI Proceedings Neogene-Quaternary Boundary and for the Establishment of the Saketi Fossil Park*, 1979, pp. 113–116, Geol. Surv. of India, Kolkata, India.
- Nelson, K. D., and Project INDEPTH Team (1998), The Himalaya and Tibetan Plateau: A perspective from project INDEPTH, paper presented at 1998 Annual Meeting, Geol. Soc. of Am., Boulder, Colo.
- Ni, J., and M. Barazangi (1984), Seismotectonics of the Himalayan collision zone: Geometry of the underthrusting Indian plate beneath the Himalaya, *J. Geophys. Res.*, *89*, 1147–1163.
- Oatney, E. M., et al. (2001), Contribution of Trans-Yamuna active fault systems towards hanging wall strain released above the décollement, Himalayan foothills of northwestern India, *Himalayan Geol.*, *22*, 9–28.
- Pandey, M. R., and P. Molnar (1988), The distribution of intensity of the Bihar-Nepal earthquake of 15 January 1934 and bounds on the extent of the rupture zone, *J. Geol. Soc. Nepal*, *5*, 22–44.
- Pandey, M. R., et al. (1995), Interseismic strain accumulation on the Himalayan crustal ramp (Nepal), *Geophys. Res. Lett.*, *22*, 751–754.
- Park, J. K., et al. (2005), Global Seismographic Network records the great Sumatra-Andaman earthquake, *Eos Trans. AGU*, *86*, 57, 60–61.
- Paul, J., et al. (2001), The motion and active deformation of India, *Geophys. Res. Lett.*, *28*, 647–650.
- Powers, P. M., et al. (1998), Structure and shortening of the Kangra and Dehra Dun reentrants, sub-Himalaya, India, *Geol. Soc. Am. Bull.*, *110*, 1010–1027.
- Raiverman, V., et al. (1993), On the foothill thrust of northwestern Himalaya, in *Himalayan Geology and Geophysics: Selected Papers Presented at the Seminar*, edited by A. C. Nanda and A. K. Dubey, pp. 237–256, Wadia Inst. of Himalayan Geol., Dehra Dun, India.
- Rao, Y. S. N., et al. (1973), Wrench-faulting and its relationship to the structure of the southern margin of the sub-Himalayan belt around Ramnagar, Uttar Pradesh, *J. Geol. Soc. India*, *14*, 249–256.
- Rao, Y. S. N., et al. (1974), On the structure of the Siwalik range between rivers Yamuna and Ganga, *Him. Geol.*, *4*, 137–150.
- Rupke, N. (1974), Stratigraphic and structural evolution of the Kumaon Lesser Himalaya, *Sediment. Geol.*, *11*, 81–265.
- Sahni, M. R., and E. Kahn (1964), Stratigraphy, structure and correlation of the Upper Siwaliks east of Chandigarh, *J. Paleontol. Soc. India*, *4*, 59–72.
- Schelling, D., and K. Arita (1991), Thrust tectonics, crustal shortening, and the structure of the far-eastern Nepal Himalaya, *Tectonics*, *10*, 851–862.
- Seeber, L., and J. Armbruster (1981), Great detachment earthquakes along the Himalayan Arc and long-term forecasting, in *Earthquake Prediction: An International Review, Maurice Ewing Ser.*, vol. 4, edited by D. W. Simpson and P. G. Richards, pp. 259–277, AGU, Washington, D. C.
- Srivastava, J. P., et al. (1981), Review of some of the recent biostratigraphic work on the Siwalik rocks of northwest Himalaya, in *GSI Proceedings Neogene-Quaternary Boundary and for the Establishment of the Saketi Fossil Park*, 1979, pp. 233–241, Geol. Surv. of India, Kolkata, India.
- Srivastava, P., and G. Mitra (1994), Thrust geometries and deep structure of the Outer and Lesser Himalaya, Kumaon and Garhwal (India): Implications for evolution of the Himalayan fold-and-thrust belt, *Tectonics*, *13*, 89–109.
- Stein, R. S., and R. S. Yeats (1989), Hidden earthquakes, *Sci. Am.*, *260*(6), 48–57.
- Stuiver, M., and H. A. Polach (1977), Discussion: Reporting of C-14 data, *Radiocarbon*, *19*, 355–363.
- Stuiver, M., and P. J. Reimer (1993), Extended (super 14) C data base and revised CALIB 3.0 (super 14) C age calibration program, *Radiocarbon*, *35*, 215–230.
- Stuiver, M., et al. (1998), INTCAL98 radiocarbon age calibration, 24,000–0 cal BP, *Radiocarbon*, *40*, 1041–1083.
- Sykes, L. R., and R. C. Quittmeyer (1981), Repeat times of great earthquakes along simple plate boundaries, in *Earthquake Prediction: An International Review*, edited by D. W. Simpson and P. G. Richards, pp. 217–247, AGU, Washington, D. C.
- Thakur, V. C. (1995), Geology of Dun Valley, Garhwal Himalaya, neotectonics and coeval deposition with fault-propagation folds, *Himalayan Geol.*, *6*, 1–8.
- Upreti, B. N., et al. (2000), The latest active faulting in southeast Nepal, in *Active Fault Research for the New Millennium*, edited by K. Okumura, K. Takada, and H. Goto, pp. 533–536, Hokudan Int. Symp. and Sch. on Active Fault, Hokudan, Awaji Island, Hyogo, Japan.
- Valdiya, K. S. (1992), The Main Boundary Thrust zone of the Himalaya, India, *Ann. Tecton.*, *6*, 54–84.
- Valdiya, K. S. (2003), Reactivation of Himalayan frontal fault: Implications, *Curr. Sci.*, *85*, 1031–1040.
- Wang, Q., et al. (2001), Present-day crustal deformation in China constrained by Global Positioning System measurements, *Science*, *294*, 574–577.
- Wesnousky, S. G., et al. (1999), Uplift and convergence along the Himalayan Frontal Thrust of India, *Tectonics*, *18*, 967–976.
- Yeats, R. S., and R. J. Lillie (1991), Contemporary tectonics of the Himalayan frontal fault system: Folds, blind thrusts and the 1905 Kangra earthquake, *J. Struct. Geol.*, *13*, 215–225.
- Yeats, R. S., and V. C. Thakur (1998), Reassessment of earthquake hazard based on a fault-bend fold model of the Himalayan plate-boundary fault, *Curr. Sci.*, *74*, 230–233.
- Yeats, R. S., et al. (1992), The Himalayan frontal fault system, *Ann. Tecton.*, *6*, suppl., 85–98.
- Zhao, W., et al. (1993), Deep seismic reflection evidence for continental underthrusting beneath southern Tibet, *Nature*, *366*, 557–559.

R. W. Briggs, S. Kumar, and S. G. Wesnousky, Center for Neotectonic Studies, University of Nevada, Reno, NV 89577, USA. (senthil@seismo.unr.edu)

R. Jayangondaperumal and V. C. Thakur, Wadia Institute of Himalayan Geology, Dehra Dun, UA 248001, India.

T. K. Rockwell, Department of Geological Sciences, San Diego State University, San Diego, CA 92182, USA.